Q. J. R. Meteorol. Soc. (1999), **125**, pp. 2535–2562

Conceptual models of upper-level frontogenesis in south-westerly and north-westerly flow

By DAVID M. SCHULTZ* and CHARLES A. DOSWELL III
National Severe Storms Laboratory, National Oceanic and Atmospheric Administration, USA

(Received 23 February 1998; revised 30 December 1998)

SUMMARY

The conceptual model proposed by Shapiro as it is applied to the evolution of an upper-level frontal zone within a baroclinic wave is reviewed and its limitations are investigated through previous literature and two case-studies presented in this paper. The early stages in the evolutions of these two cases are used to examine specific limitations of this conceptual model: (1) upper-level frontogenesis in south-westerly flow that evolves from a state of equivalent barotropy to a state of cold advection along the front, and (2) upper-level frontogenesis in north-westerly flow with along-front variation in the sign of the thermal advection, such that warm advection occurs upstream of cold advection in the thermal trough.

Vector-frontogenesis diagnostics for the Lagrangian rate of change of the magnitude and direction of the horizontal potential-temperature gradient, including tilting due to vertical motion, are derived. These diagnostics are applied to the two cases to examine the maintenance of the potential-temperature gradient and the development of cold advection along each upper-level front. The upper-level front in south-westerly (north-westerly) flow was maintained primarily by deformation (tilting) frontogenesis, in agreement with previous research. The increasing cold advection along the upper-level front in both cases was related to an upstream vorticity maximum. For the case in south-westerly flow, the pre-existing vorticity maximum approached a downstream equivalent-barotropic upper-level front in a manner similar to an instant occlusion, resulting in cold advection along the length of the upper-level front. For the case in north-westerly flow, an intensifying vorticity maximum concentrated the cold advection in the base of the thermal trough, as warm advection developed upstream.

These two cases are compared to upper-level fronts in previous literature and a climatology of upper-level fronts associated with landfalling cyclones over the eastern North Pacific Ocean. The results indicate that these two cases are typical of early evolutions of upper-level fronts that can occur in south-westerly and north-westerly flow. Therefore, a revised version of the Shapiro conceptual model is presented that represents more accurately the early evolutions exhibited in the present and previous studies.

KEYWORDS: Atmospheric dynamics Fronts Shapiro effect

1. INTRODUCTION

As noted in the review by Keyser and Shapiro (1986), baroclinic zones in the upper troposphere and lower stratosphere associated with the polar-front jet stream (known as upper-level fronts) apparently were observed first by Bjerknes and Palmén (1937). More studies followed that examined the structure and dynamics of upper-level fronts in more detail (e.g. Palmén and Nagler 1949; Berggren 1952; Newton and Carson 1953; Reed and Sanders 1953; Newton 1954; Reed 1955; Reed and Danielsen 1959; Staley 1960; Newton and Persson 1962; Danielsen 1964; Newton 1965; Bosart 1970; Shapiro 1970). The results from this early research can be summarized as follows. (1) Upper-level fronts are typically narrow (~100 km) in the cross-front direction and extend downward from the tropopause, often associated with stratospheric air, as indicated by high values of potential vorticity and ozone mixing ratio. (2) These upper-level fronts are typically related to regions of localized maxima of wind speed (i.e. jet streaks, as first defined by Newton and Carson (1953, p. 325); hence these systems are sometimes also referred to as upper-level jet–front systems). (3) In most cases, the intensification of the horizontal potential-temperature gradient within these upper-level fronts (i.e. frontogenesis) and the vertical extent of the baroclinicity are attributed primarily to isentropic tilting by horizontal gradients of vertical motion (i.e. subsidence, maximized on the warm side of the upper-level front, leads to frontogenesis). In other cases, upper-level frontogenesis can occur due to horizontal confluent deformation,

* Corresponding author: NOAA/National Severe Storms Laboratory, 1313 Halley Circle, Norman, OK 73069, USA. e-mail: schultz@nssl.noaa.gov

with tilting being frontolytic. (4) Although examples of strong frontogenesis in south-westerly flow are known to occur (e.g. Reed 1955; Bosart 1970), the most intense upper-level frontogenesis tends to occur with systems forming in north-westerly flow, where the differential subsidence across the upper-level front is greatest. This last point was later demonstrated by modelling studies based on real and idealized upper-level fronts (e.g. Shapiro 1981; Keyser and Pecnick 1985; Keyser *et al.* 1986; Reeder and Keyser 1988): synoptic-scale confluence at a jet-entrance region and cold advection along the length of the front yield a gradient in vertical motion across the upper-level front of sufficient magnitude to produce frontogenesis. (The effect of both confluence and cold advection during upper-level frontogenesis has been referred to as *the Shapiro effect* (Rotunno *et al.* 1994).)

(*a*) *The Shapiro conceptual model*

As noted by Keyser and Shapiro (1986, p. 466), data limitations of these early observational studies were primarily responsible for previous ambiguities and inconsistencies in understanding the dynamical interactions between the primary and secondary circulations in upper-level frontal systems. In an effort to link secondary circulations calculated from the Sawyer–Eliassen equation in two-dimensional models with three-dimensional circulations calculated from observational data, Shapiro (1982, Fig. 7) created a schematic of the movement 'of an upper-tropospheric jet–front system through a midlatitude baroclinic wave' (Shapiro and Keyser 1990, Fig. 10.8 caption), emphasizing the typical thermal-advection pattern for one such life cycle associated with these systems. Although this schematic (Fig. 1; hereafter, the Shapiro conceptual model) was not meant to address the issue of upper-level frontogenesis directly, Lagrangian frontogenesis is implied at different stages in the progression of the jet–front system through the baroclinic wave.

Despite the Shapiro conceptual model not having been designed to illustrate frontogenesis directly, the schematic has become firmly entrenched in later scientific literature, attesting to its success in describing many of the general features of the migration of an upper-level jet–front system through a larger-scale baroclinic wave. The schematic has been reproduced in review articles on upper-level fronts (e.g. Keyser and Shapiro 1986, Fig. 19; Shapiro and Keyser 1990, Fig. 10.8) and emulated in textbooks (e.g. Carlson 1991, Fig. 15.6; Bluestein 1993, Fig. 2.82). Despite the successes of the Shapiro conceptual model in interpretation of the secondary circulations at different stages in the life cycle of a baroclinic wave, applications of the Shapiro schematic to frontogenesis, however, appear to be an oversimplification of the structural and kinematic complexities inherent in nature (as discussed later). The present study endeavours to consider some of these complexities.

The Shapiro conceptual model begins with an upper-level front situated within confluent north-westerly flow (e.g. Namias and Clapp 1949), and isentropes are nearly parallel to isohypses (Fig. 1(a)). This phase of the evolution will be referred to hereafter as the *equivalent-barotropic stage*. Approximately 24 h later, the front evolves to a state where the trough in the isentropes lags the trough in the isohypses, implying geostrophic cold advection along the length of the front (the *cold-advection stage*; Fig. 1(b)). Later, the trough in the geopotential-height field closes off and becomes more symmetrical (the *closed-low stage*; Fig. 1(c)), as discussed by Bell and Keyser (1993) and Bell and Bosart (1994), with leading warm advection and trailing cold advection. Finally, the closed low opens up in confluent south-westerly flow and geostrophic warm advection along the length of the front is implied (the *warm-advection stage*; Fig. 1(d)).

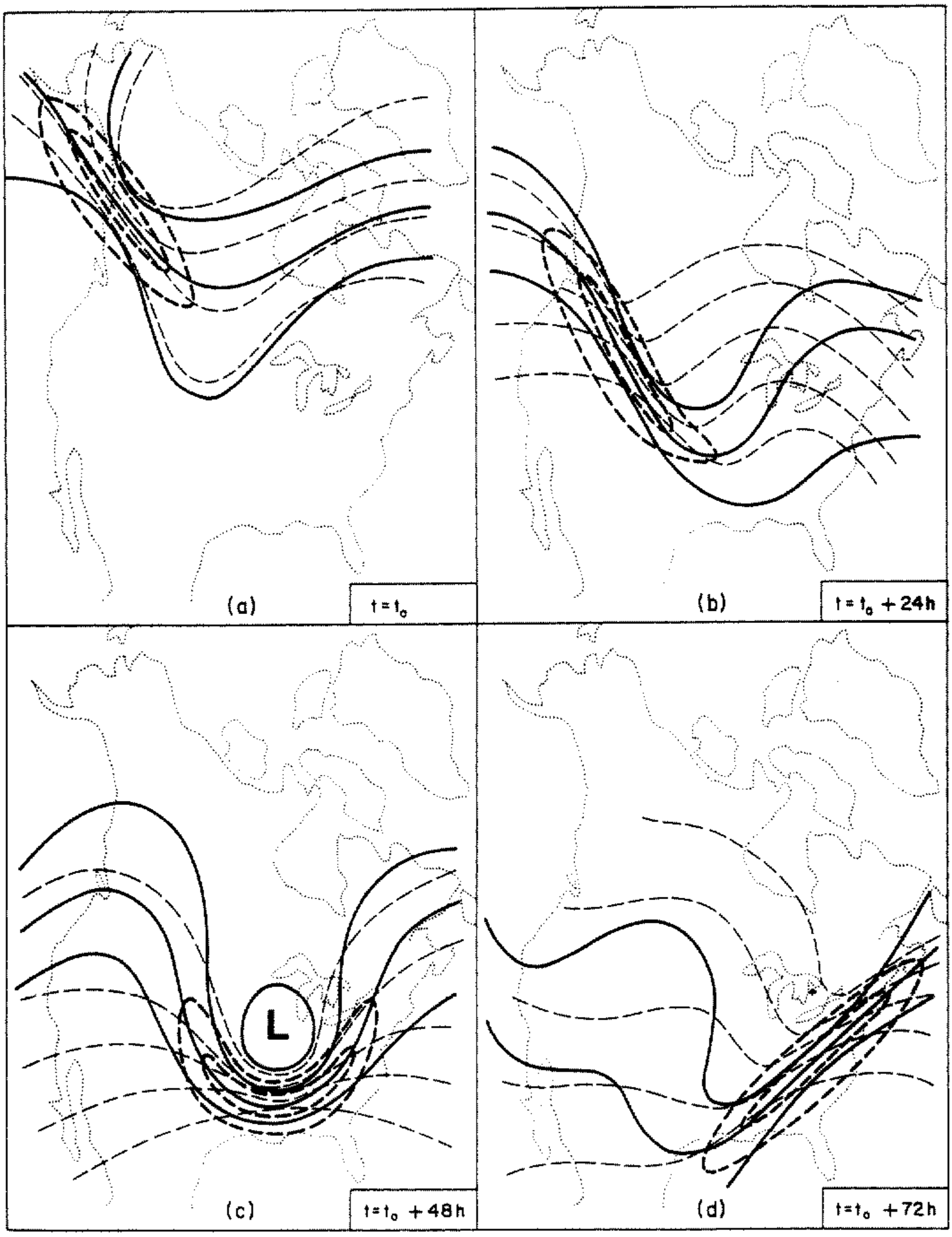

Figure 1. Idealized schematic depiction, on an upper-tropospheric isobaric surface, of the evolution of an upper-level jet–front system through a mid-latitude baroclinic wave over a 72-h period: (a) formation of the jet–front system in the confluence between the mid- and high-latitude currents; (b) jet–front system situated in the north-westerly flow inflection of amplifying wave; (c) jet–front system at the base of the trough of fully developed wave; (d) jet–front system situated in the south-westerly flow inflection of damping wave. Geopotential height contours, thick solid lines; isotachs, thick dashed lines; isentropes or isotherms, thin dashed lines. From Shapiro (1982, Fig. 7).

TABLE 1. CASES OF UPPER-LEVEL FRONTS THAT DEVIATE FROM THE SHAPIRO CONCEPTUAL MODEL (SEE TEXT) WITH STRONG COLD ADVECTION IN THE BASE OF THE TROUGH AND/OR WARM ADVECTION IN THE TRAILING RIDGE

Palmén and Nagler (1949)	Figs. 1 and 2
Reed and Sanders (1953)	Figs. 1 and 2
Newton (1954)	Figs. 3 and 4
Reed (1955)	Figs. 5 and 6
Newton (1958)	Figs. 2 and 4
Staley (1960)	Figs. 2 and 3
Newton and Palmén (1963)	Fig. 3
Shapiro (1976)	Figs. 15 and 16
Sanders (1988)	Figs. 9 and 10
Neiman and Shapiro (1989)	Figs. 4, 9, and 12
Sanders *et al.* (1991)	pp. 1364–1365
Djurić (1994)	Fig. 8-18
Lackmann *et al.* (1997)	Figs. 12(a),(c)
Pyle (1997)	p. 64, Fig. 23(d)

Although it appears as if the intent of the Shapiro conceptual model was to illustrate the evolution of a jet–front system (e.g. '$t = t_0$', '$t = t_0 + 24$ h', etc. in Fig. 1), observational evidence suggests that this schematic evolution typically does not occur exactly in the manner illustrated by Shapiro (1982), particularly over North America. First, cold advection is depicted as maximum at the inflection point in the height field in the cold-advection stage of the Shapiro conceptual model with negligible thermal advection outside of the frontal zone. Nearly all observed upper-level fronts in north-westerly flow in the literature, however, exhibit the strongest cold advection in the base of the thermal trough (Table 1). Weak cold advection, or more typically warm advection, is present along the north-westerly extensions of the fronts (Table 1). Second, as noted by Newton and Carson(1953, p. 325), Newton and Palmén (1963), Cammas and Ramond (1989, p. 2460), Orlanski and Sheldon (1995, Fig. 3, p. 614) and Pyle (1997, pp. 97 and 133), the progression of a jet–front structure from north-westerly flow to the base of the trough to south-westerly flow (Figs. 1(b)–(d)) rarely exists. Since the wind speed within a jet streak is usually much faster than the speed of movement of the jet streak (e.g. Newton and Carson 1953, p. 331; Palmén and Newton 1969, pp. 206 and 207; Cunningham and Keyser 1996, section 3), the jet–front system cannot be tracked as an advective feature of the flow. Often, as a new jet–front system is developing in the downstream south-westerly flow, the upstream jet–front system in north-westerly flow remains. A further point is that the reorganization from large-scale diffluence during the cold-advection stage to large-scale confluence during the warm-advection stage (cf. Figs. 1(b) and (d)) seems unlikely to occur within the relatively short time period depicted by the Shapiro conceptual model. Finally, the Shapiro conceptual model illustrates the evolution of an upper-level front in north-westerly flow, although as will be shown later in this paper, upper-level fronts in south-westerly flow also may display some similarities (e.g. evolution from equivalent-barotropic to cold-advection stages) to the Shapiro conceptual model at times.

(*b*) *Purpose*

The purpose of this paper, therefore, is to compare and contrast the early evolution of south-westerly and north-westerly flow upper-level frontogenesis, using two cases as illustrative examples. Specifically, we intend to demonstrate the following points. First, the kinematics and dynamics differ for upper-level fronts in south-westerly and

north-westerly flow and have not been elucidated previously for pure south-westerly flow upper-level frontogenesis. Second, the mechanism that leads to the initiation and configuration of strong cold advection along observed upper-level fronts has not been determined. Understanding this mechanism is of importance because cold advection along upper-level fronts is concomitant with stronger tilting and upper-level frontogenesis (the Shapiro effect), processes that can be associated with surface cyclogenesis (e.g. Uccellini *et al.* 1985, pp. 980 and 981). Finally, south-westerly flow upper-level frontogenesis appears to be common over the eastern North Pacific Ocean, in contrast to north-westerly flow frontogenesis, which appears to be common over North America.

Section 2 is a derivation of vector frontogenesis, including the vertical-velocity (tilting) terms. Section 3 introduces the two cases of upper-level frontogenesis in south-westerly and north-westerly flow, respectively. Then, the changes in the magnitude and direction of the horizontal potential-temperature gradient along the two upper-level fronts are diagnosed using vector frontogenesis. Section 4 is a climatology of upper-level fronts associated with landfalling cyclones on the west coast of North America, showing that evolutions similar to that occurring in south-westerly flow are not an uncommon occurrence. Finally, section 5 presents a concluding discussion and a revised conceptual model for the early evolution of south-westerly and north-westerly flow upper-level frontogenesis.

2. Derivation of the two-dimensional vector frontogenesis, including vertical-velocity terms

As originally defined by Petterssen (1936) for surface fronts, frontogenesis is the Lagrangian rate of change of the magnitude of the horizontal potential-temperature (θ) gradient due to the horizontal wind ($\mathbf{V}_\mathrm{H} = u\mathbf{i} + v\mathbf{j}$). Miller (1948) extended Petterssen's definition to fronts in the free atmosphere by defining frontogenesis as the Lagrangian rate of change of the magnitude of the three-dimensional gradient of the potential temperature due to the three-dimensional wind ($\mathbf{V} = \mathbf{V}_\mathrm{H} + \omega\mathbf{k} = u\mathbf{i} + v\mathbf{j} + \omega\mathbf{k}$), written here in ($x$, y, p) coordinates. In this paper, we wish to understand the evolution of an upper-level front from a state of near equivalent barotropy to a state of cold advection along the front, involving the rotation of isentropes relative to isohypses. This reconfiguration of the isentropes suggests that a useful diagnostic would be the vector-frontogenesis formulation of Keyser *et al.* (1988), which considers the Lagrangian rate of change of the magnitude *and direction* of the horizontal potential temperature gradient by the horizontal wind. Since contributions from vertical motion are typically small for surface fronts, but not necessarily so for upper-level fronts, we extend Keyser *et al.*'s (1988) methodology to include the frontogenetical effects due to vertical motion. (A similar derivation can be found in Lalaurette *et al.* (1994, pp. 2005–2007).) Therefore, for the purposes of this paper, we define vector frontogenesis, $\mathbf{F}$, as the Lagrangian rate of change of the magnitude and direction of the *horizontal* potential temperature gradient due to the *three-dimensional* wind:

$$\mathbf{F} = \frac{\mathrm{d}}{\mathrm{d}t}\nabla_\mathrm{H}\theta, \tag{1}$$

where

$$\frac{\mathrm{d}}{\mathrm{d}t} = \frac{\partial}{\partial t} + u\frac{\partial}{\partial x_\mathrm{p}} + v\frac{\partial}{\partial y_\mathrm{p}} + \omega\frac{\partial}{\partial p},$$

$$\nabla_\mathrm{H} = \mathbf{i}\frac{\partial}{\partial x_\mathrm{p}} + \mathbf{j}\frac{\partial}{\partial y_\mathrm{p}}.$$

The subscript p indicates differentiation on an isobaric surface and hereafter will be implicit in this section. Resolving **F** into natural coordinates (s, n) such that the s axis is locally tangent to an isentrope and the n axis points towards colder air on a constant pressure surface (i.e. **s** points in the same direction as the thermal wind):

$$\frac{\mathrm{d}}{\mathrm{d}t}\nabla_{\mathrm{H}}\theta = \mathbf{n}\left(\mathbf{n}\cdot\frac{\mathrm{d}}{\mathrm{d}t}\nabla_{\mathrm{H}}\theta\right) + \mathbf{s}\left(\mathbf{s}\cdot\frac{\mathrm{d}}{\mathrm{d}t}\nabla_{\mathrm{H}}\theta\right), \tag{2}$$

where

$$\mathbf{n} = -|\nabla_{\mathrm{H}}\theta|^{-1}\nabla_{\mathrm{H}}\theta, \tag{3a}$$

$$\mathbf{s} = \mathbf{n}\times\mathbf{k}. \tag{3b}$$

Equation (1) becomes

$$\mathbf{F} = F_n\mathbf{n} + F_s\mathbf{s}, \tag{4}$$

where F_n is referred to as the scalar frontogenesis and F_s is referred to as the rotational frontogenesis (Keyser *et al.* 1988, Eqs. (2.3a) and (2.3b)):

$$F_n = -\frac{\mathrm{d}}{\mathrm{d}t}|\nabla_{\mathrm{H}}\theta|, \tag{5a}$$

$$F_s = \mathbf{n}\cdot\left(\mathbf{k}\times\frac{\mathrm{d}}{\mathrm{d}t}\nabla_{\mathrm{H}}\theta\right). \tag{5b}$$

Therefore, positive F_n implies frontolysis, whereas positive F_s implies cyclonic rotation of the isentropes.

Conservation of potential temperature in three-dimensional adiabatic flow means that

$$\frac{\partial\theta}{\partial t} + \mathbf{V}\cdot\nabla\theta = 0, \tag{6}$$

where

$$\nabla = \mathbf{i}\frac{\partial}{\partial x} + \mathbf{j}\frac{\partial}{\partial y} + \mathbf{k}\frac{\partial}{\partial p}.$$

Following Keyser *et al.* (1988, p. 764), differentiating (6) respectively by x and y yields:

$$\frac{\mathrm{d}}{\mathrm{d}t}\left(\frac{\partial\theta}{\partial x}\right) = -\frac{\partial u}{\partial x}\frac{\partial\theta}{\partial x} - \frac{\partial v}{\partial x}\frac{\partial\theta}{\partial y} - \frac{\partial\omega}{\partial x}\frac{\partial\theta}{\partial p}, \tag{7a}$$

$$\frac{\mathrm{d}}{\mathrm{d}t}\left(\frac{\partial\theta}{\partial y}\right) = -\frac{\partial u}{\partial y}\frac{\partial\theta}{\partial x} - \frac{\partial v}{\partial y}\frac{\partial\theta}{\partial y} - \frac{\partial\omega}{\partial y}\frac{\partial\theta}{\partial p}. \tag{7b}$$

Equations (5a) and (5b) can be rewritten:

$$F_n = -\frac{1}{|\nabla_{\mathrm{H}}\theta|}\left\{\frac{\partial\theta}{\partial x}\frac{\mathrm{d}}{\mathrm{d}t}\left(\frac{\partial\theta}{\partial x}\right) + \frac{\partial\theta}{\partial y}\frac{\mathrm{d}}{\mathrm{d}t}\left(\frac{\partial\theta}{\partial y}\right)\right\}, \tag{8a}$$

$$F_s = -\frac{1}{|\nabla_{\mathrm{H}}\theta|}\left\{\frac{\partial\theta}{\partial y}\frac{\mathrm{d}}{\mathrm{d}t}\left(\frac{\partial\theta}{\partial x}\right) - \frac{\partial\theta}{\partial x}\frac{\mathrm{d}}{\mathrm{d}t}\left(\frac{\partial\theta}{\partial y}\right)\right\}. \tag{8b}$$

Combining (7a) and (7b) with (8a) and (8b) leads to the following expressions:

$$F_n = -\frac{1}{|\nabla_H \theta|}\left\{\underbrace{\frac{\partial\theta}{\partial x}\left(-\frac{\partial u}{\partial x}\frac{\partial\theta}{\partial x}-\frac{\partial v}{\partial x}\frac{\partial\theta}{\partial y}\right)}_{n_1}+\underbrace{\frac{\partial\theta}{\partial y}\left(-\frac{\partial u}{\partial y}\frac{\partial\theta}{\partial x}-\frac{\partial v}{\partial y}\frac{\partial\theta}{\partial y}\right)}_{n_2}\right.$$
$$\left.+\underbrace{\frac{\partial\theta}{\partial p}\left(-\frac{\partial\omega}{\partial x}\frac{\partial\theta}{\partial x}-\frac{\partial\omega}{\partial y}\frac{\partial\theta}{\partial y}\right)}_{n_3}\right\}, \tag{9a}$$

$$F_s = -\frac{1}{|\nabla_H \theta|}\left\{\underbrace{\frac{\partial\theta}{\partial y}\left(-\frac{\partial u}{\partial x}\frac{\partial\theta}{\partial x}-\frac{\partial v}{\partial x}\frac{\partial\theta}{\partial y}\right)}_{s_1}-\underbrace{\frac{\partial\theta}{\partial x}\left(-\frac{\partial u}{\partial y}\frac{\partial\theta}{\partial x}-\frac{\partial v}{\partial y}\frac{\partial\theta}{\partial y}\right)}_{s_2}\right.$$
$$\left.+\underbrace{\frac{\partial\theta}{\partial p}\left(\frac{\partial\omega}{\partial y}\frac{\partial\theta}{\partial x}-\frac{\partial\omega}{\partial x}\frac{\partial\theta}{\partial y}\right)}_{s_3}\right\}. \tag{9b}$$

Terms n_1, n_2, s_1, and s_2 represent similar terms in Keyser *et al.*'s (1988) derivation. Term n_3 represents tilting scalar frontogenesis due to vertical-velocity gradients acting on the horizontal potential-temperature gradient (equivalent to the sum of terms 4 and 8 in Bluestein (1986, p. 181; 1993, p. 253)) and term s_3 represents tilting rotational frontogenesis due to vertical-velocity gradients acting on the horizontal potential-temperature gradient.* Terms n_3 and s_3 can also be expressed as:

$$n_3 = -\frac{\partial\theta}{\partial p}(\nabla_H\omega\cdot\nabla_H\theta)$$
$$= -\frac{\partial\theta}{\partial p}\left(\frac{\partial\omega}{\partial n}\right), \tag{10a}$$

$$s_3 = -\frac{\partial\theta}{\partial p}\mathbf{k}\cdot(\nabla_H\omega\times\nabla_H\theta)$$
$$= -\frac{\partial\theta}{\partial p}\left(\frac{\partial\omega}{\partial s}\right), \tag{10b}$$

respectively. These expressions for n_3 and s_3 exhibit the behaviour that when $\nabla_H\omega$ is in the same direction as $\nabla_H\theta$, the tilting scalar frontogenesis, n_3, is maximized, but the tilting rotational frontogenesis, s_3, is zero (Fig. 2(a)). In contrast, when $\nabla_H\omega$ is perpendicular to $\nabla_H\theta$, n_3 is zero, but $|s_3|$ is maximized (Fig. 2(b)).

* A similar expression for 'tilting scalar frontogenesis' in an x–z plane, involving v_{ag}, the ageostrophic cross-front wind, can be found in Keyser *et al.* (1986, Eq. (2.12)).

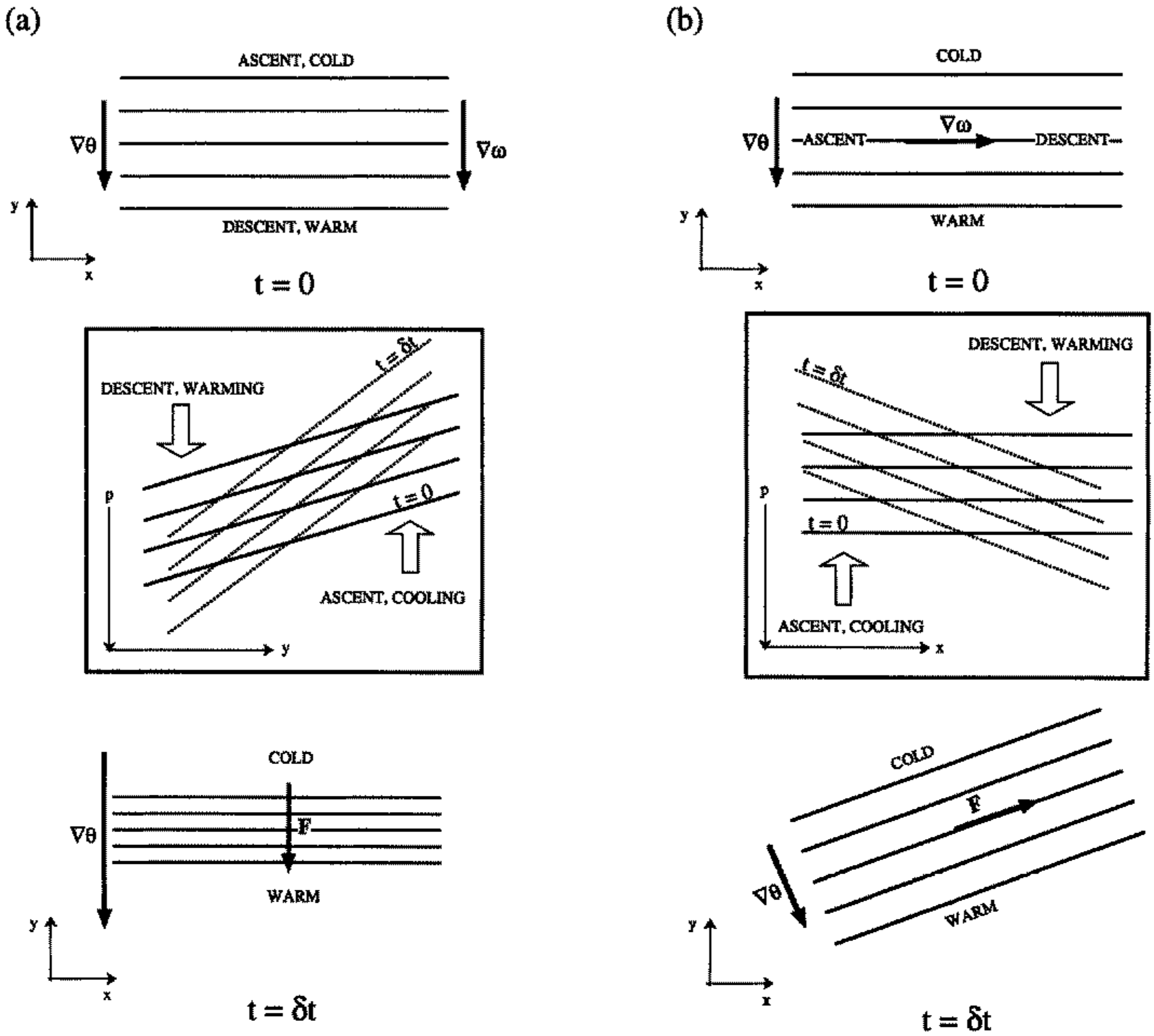

Figure 2. Schematic illustrating vertical tilting terms in the expression for vector frontogenesis of the horizontal potential-temperature gradient. Solid lines are isentropes at two times ($t = 0$ and $t = \delta t$). Vectors are labelled. Insets: Solid lines are isentropes at $t = 0$ and dashed lines are isentropes at $t = \delta t$. Open arrows represent vertical motions. (a) Tilting scalar frontogenesis: $\nabla_H\omega$ and $\nabla_H\theta$ in the same direction such that n_3 is maximized and $\nabla_H\omega \times \nabla_H\theta = 0$. F is therefore in the direction of $\nabla_H\theta$. (b) Tilting rotational frontogenesis: $\nabla_H\omega$ and $\nabla_H\theta$ perpendicular such that $|s_3|$ is maximized and $\nabla_H\omega \cdot \nabla_H\theta = 0$. F is therefore perpendicular to $\nabla_H\theta$.

Following Keyser *et al.* (1988, pp. 764 and 765), expressions similar to their eqs. (2.10a) and (2.10b) result:

$$F_n = \frac{1}{2}|\nabla_H\theta|(\nabla_H \cdot \mathbf{V}_H - E\cos 2\beta) - \frac{\partial\theta}{\partial p}(\nabla_H\omega \cdot \nabla_H\theta), \tag{11a}$$

$$F_s = \frac{1}{2}|\nabla_H\theta|(\mathbf{k} \cdot \nabla_H \times \mathbf{V}_H + E\sin 2\beta) - \frac{\partial\theta}{\partial p}\mathbf{k} \cdot (\nabla_H\omega \times \nabla_H\theta), \tag{11b}$$

where E is the resultant deformation and β is the local angle between an isentrope and the axis of dilatation. Equation (11a) is comparable to similar expressions in Saucier (1955, pp. 363–365). This expression for F_n comprises three terms related to divergence, deformation, and tilting, whereas (11b) for F_s comprises three terms related to relative

vorticity, deformation, and tilting. These partitions will be useful for examining the evolution of the fronts in the two observed cases.*

3. Case studies

In this section, we present two case studies of the early stages in the evolution of upper-level fronts, in south-westerly and north-westerly upper-level flow, respectively. Section 3(a) describes the mesoscale-model simulation used to examine these two cases, which are introduced in section 3(b). The cases are further analyzed in section 3(c) using the vector-frontogenesis diagnostics developed in section 2.

(*a*) *Mesoscale-model description*

The Pennsylvania State University–National Center for Atmospheric Research (PSU–NCAR) mesoscale model version 5 (MM5), a nonhydrostatic, primitive-equation, σ-coordinate model (Dudhia 1993; Grell *et al.* 1994), was employed to simulate the two upper-level frontogenesis events. Since both the south-westerly and north-westerly flow events occurred nearly simultaneously, one simulation was able to accommodate analysis of both. The simulation was initialized at 1200 UTC 12 December 1988, was ended at 1200 UTC 14 December 1988, and features 23, variably spaced, half-σ levels in the vertical. A 30 km horizontal-resolution domain was nested within a 90 km horizontal-resolution domain using a two-way interactive mesh-refinement scheme. Precipitation processes were parametrized using an explicit moisture scheme that includes prognostic equations for water vapour, cloud-water, rain-water, cloud-ice, and snow (Dudhia 1989; Grell *et al.* 1994, section 5.3.1.1). The Kain–Fritsch cumulus parametrization (Kain and Fritsch 1993) was used to represent subgrid-scale convective precipitation. Other parametrizations included a multilevel planetary boundary layer (Zhang and Anthes 1982) and a radiative upper-boundary condition (Klemp and Durran 1983).

Four-dimensional data assimilation was used throughout the simulation on the 90 km domain and during the first 12 h on the 30 km domain. The assimilation technique (Stauffer and Seaman 1990) employed Newtonian nudging to relax the model simulation to gridded 12 h upper-level and 3 h surface analyses. To create the upper-level analyses, National Meteorological Center (NMC, now known as the National Centers for Environmental Prediction) analyses were interpolated to the model grid. Surface and upper-air observations were then incorporated into the analysis using a Cressman-type analysis scheme (Benjamin and Seaman 1985). After the removal of superadiabatic lapse rates below 500 hPa, the analysis was interpolated to the σ-coordinate system, and the integrated mean divergence was removed to avoid the production of spurious gravity waves. Three-hour surface analyses were generated similarly, with first-guess analysis fields provided by linear interpolation of 12 h NMC analyses. Lateral boundary conditions for the 90 km domain were generated by linear interpolation of the 12 h analyses. Throughout this paper, only output from the 90 km domain is displayed.

(*b*) *Overview*

The first case is the upper-level front associated with the landfalling Pacific cyclone over western North America on 12–13 December 1988. Our analyses are carried out at

* Strictly speaking, the rotational frontogenesis does not describe the time rate of change of the angle between isohypses and isotherms, as the height field, as well as the thermal field, will be altered by the relative vorticity, deformation, and tilting terms. Rigorous resolution of this discrepancy, however, would involve inversion techniques, the methodology for which has not matured. Nevertheless, our results suggest that the rotation of the isohypses by the vorticity is a secondary effect, at least in the cases presented here.

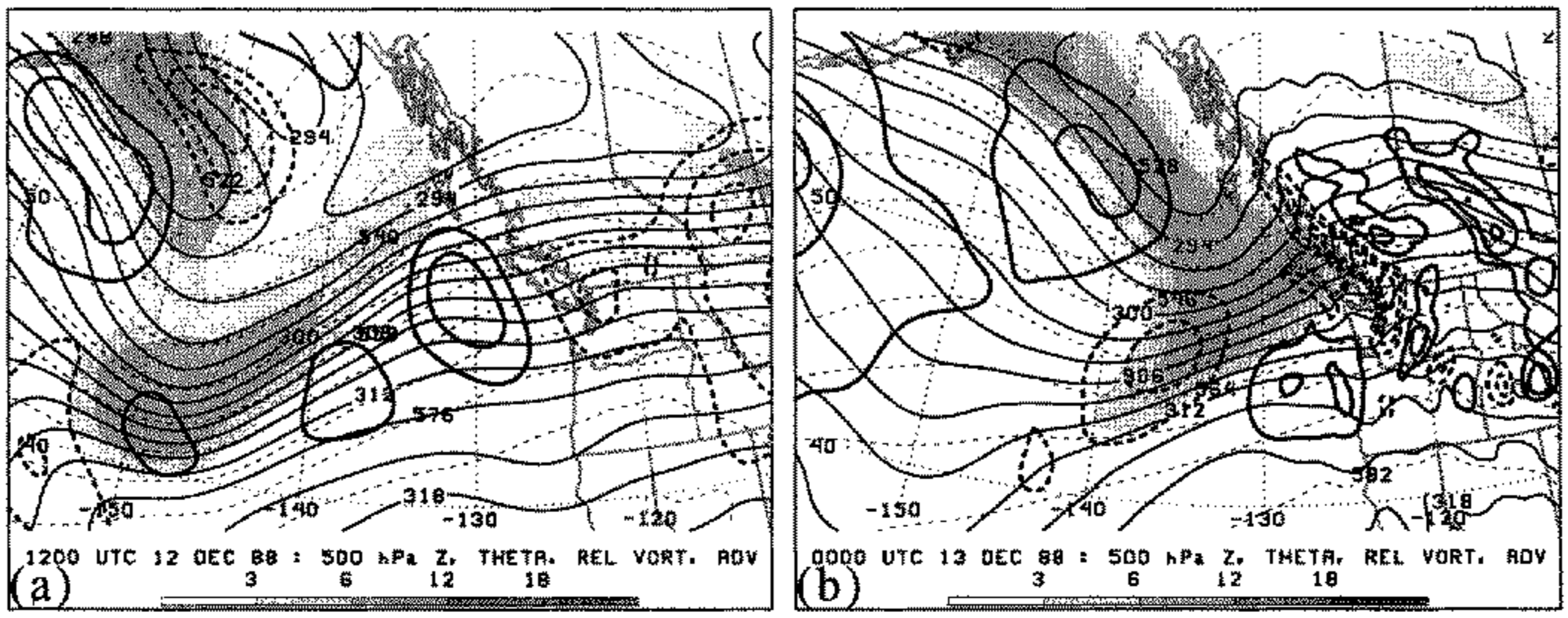

Figure 3. SW (see text) 500 hPa geopotential height (thin dashed lines every 6 dm), relative vorticity of total horizontal wind (10^{-5} s^{-1}, shaded according to scale at bottom of figure), potential temperature (thin solid lines every 2 K), and potential-temperature advection by the total horizontal wind (thick solid (dashed) lines every 12×10^{-5} K s^{-1}, from -36 to 36×10^{-5} K s^{-1}, represent warm (cold) advection): (a) 1200 UTC 12 December 1988; (b) 0000 UTC 13 December 1988.

500 hPa, a common midtropospheric level analyzed by synoptic meteorologists. While our results would be quantitatively different at upper-tropospheric levels (say, 400 or 300 hPa), our results would not differ qualitatively were another level to be presented.

Unlike other cases of upper-level fronts in south-westerly flow that apparently evolved from a north-westerly flow regime (e.g. Reed 1955; Bosart 1970; Sanders *et al.* 1991; Pyle 1997, p. 133), this case occurred entirely within south-westerly flow, and will hereafter be referred to as SW. SW was associated with a 500 hPa closed low that moved slowly into the Gulf of Alaska on 11 December 1988 (not shown). NMC analyses (not shown) indicate remnant baroclinicity on the south-east side of the closed low in south-westerly flow, with the geopotential-height (hereafter, height) and potential-temperature contours nearly parallel from 0000 UTC 11 December 1988 to 1200 UTC 12 December 1988 (hereafter 12/12) (Fig. 3(a)). Unlike the equivalent-barotropic stage in the Shapiro conceptual model (Fig. 1(a)), however, the upper-level front was strongest in the south-westerly, not the north-westerly, geostrophic flow. The enhanced baroclinicity in SW was also associated with a pre-existing progressive relative-vorticity (hereafter, vorticity) maximum at the base of the short-wave trough, coincident with the thermal trough at this level (Fig. 3(a)). Twelve hours later (13/00; Fig. 3(b)), the orientation between the isentropes and isohypses implied geostrophic cold advection (potential-temperature advection due to total horizontal wind contoured in thick lines) along much of the length of the 500 hPa front. This structure represents the cold-advection stage. Therefore, this case illustrates the same evolution from a nearly equivalent-barotropic stage to a cold-advection stage as in the Shapiro conceptual model (Figs. 1(a),(b)), except in south-westerly, instead of north-westerly, flow. It is curious to note that Hines and Mechoso (1991, Figs. 3–5) simulated a similar structure in their idealized model of primitive-equation upper-level frontogenesis: cold advection along a baroclinic zone developing in south-westerly flow. Further investigation of this case was abandoned because 'This simulated frontogenesis, therefore, has substantial differences with the observed phenomena (as characterized by the Shapiro conceptual model) and will not be analyzed further in this paper' (Hines and Mechoso 1991, p. 1232).

Satellite imagery for SW (Fig. 4) shows that a comma cloud is associated with the advection of 500 hPa cyclonic vorticity and the polar-front cloud band is associated

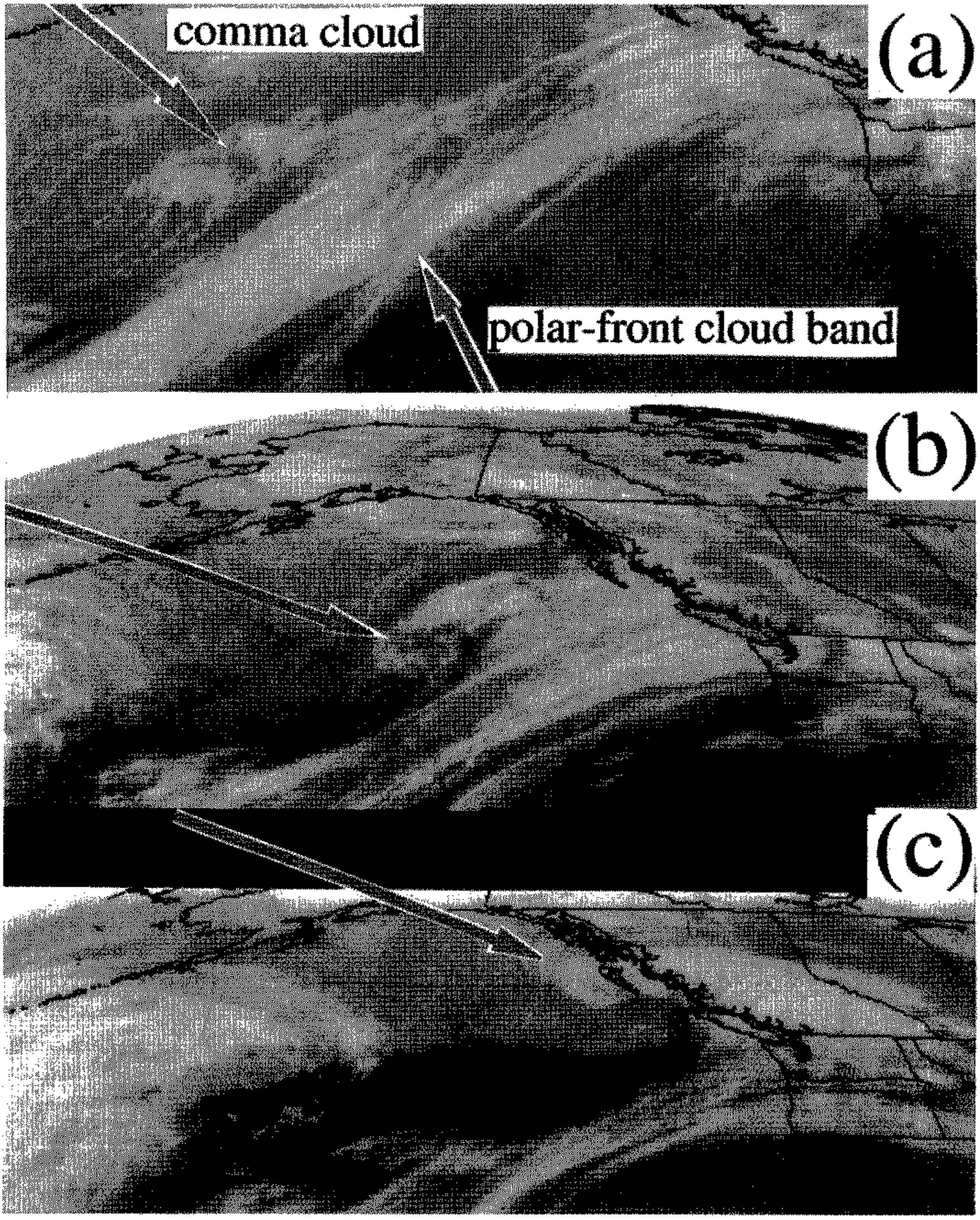

Figure 4. GOES (Global Operational Environmental Satellite)-6 infrared satellite images; arrows point to cloud features described in text: (a) 0016 UTC 12 December 1988, (b) 1216 UTC 12 December 1988, (c) 2316 UTC 12 December 1988.

with the baroclinic zone in south-westerly flow (Fig. 4(a)). As the comma cloud approaches and merges with the polar-front cloud band, the clouds deform owing to the rotation associated with the vorticity maximum (Figs. 4(b),(c)). This evolution is remarkably similar to the instant-occlusion concept reviewed by Schultz and Mass (1993, section 2(d)) and described by, for example, McGinnigle *et al.* (1988, Fig. 7(a)), Evans *et al.* (1994), and Bader *et al.* (1995, section 4.4, Figs. 4.4.3(c) and 4.4.5(c)). In particular, the approach of a short-wave trough (comma cloud) toward a pre-existing baroclinic zone in south-westerly flow (polar-front cloud band) epitomizes the instant occlusion. SW is consistent with these previous studies, in that observed instant occlusions tend to occur in confluent large-scale flows that favour merger between the comma cloud and the polar-front cloud band. As has been noted by the authors mentioned earlier, not all cyclone events that occur in south-westerly flow, however, are instant occlusions.

The other case is the upper-level front associated with the Experiment on Rapidly Intensifying Cyclones over the Atlantic (ERICA) Intensive Observing Period (IOP) 2 cyclone on 13–14 December 1988 over central North America. Because the upper-level front intensified in north-westerly upper-level flow, this case will hereafter be referred to as NW. The ERICA IOP 2 cyclone and its upper-level features have been discussed previously by Sanders (1990), Roebber (1993), Hakim (1997, section 5.1), Lackmann *et al.* (1997) and Reed and Albright (1997). At 13/00 (Fig. 5(a)), as well as 12 and 24 h previously (not shown), much of the frontal zone was characterized by weak cold advection, with the strongest cold advection on the equatorward side of the front and near the intensifying vorticity maximum. Lackmann *et al.* (1997) determined that the tilting of horizontal vorticity into the vertical by differential subsidence across the upper-level front was responsible for the formation and intensification of this vorticity maximum, which would later be associated with the ERICA IOP 2 cyclogenesis. By 13/12, however, warm advection was occurring along much of the length of the upper-level front (Fig. 5(b)). Unlike in SW, where cold advection occurred along the length of the front, the cold advection in NW was limited to the base of the thermal trough (cf. Figs. 3(b) and 5(b)) associated with the 'compacting' vorticity maximum (Lackmann *et al.* 1997). A compacting vorticity maximum is one that undergoes an increase in isotropy during its evolution (i.e. the length of the major axis of the vorticity maximum decreases relative to that of the minor axis) (Lackmann *et al.* 1997, p. 2731). Therefore, NW, as well as other similar events from the literature discussed previously, indicates significant along-front variability in thermal advection as the upper-level front reaches maturation, in contrast to the depicted cold advection dominating the entire length of the front in the Shapiro conceptual model (Fig. 1(b)).

It is apparent that significant differences exist between the early stages in the evolutions of the two cases of upper-level frontogenesis being discussed, SW and NW (Figs. 3 and 5, respectively). In particular, the evolution from the equivalent-barotropic stage to cold-advection stage in SW occurred in south-westerly, not north-westerly flow. Also, NW experienced significant along-front variation in the sign of the thermal advection, with cold advection at the leading edge of the vorticity maximum and warm advection along the north-western portion, rather than cold advection along the length of the front as portrayed in the Shapiro conceptual model (Fig. 1). It might be argued that cases exhibiting these same evolutions may be relatively uncommon, or alternatively, it may be that the Shapiro conceptual model applies best to cases in a limited geographical area (e.g. over North America). As will be shown in section 4, evolutions similar to SW are commonly associated with North Pacific cyclones landfalling on the west coast of North America, which, in turn, resemble cases throughout the northern hemisphere; we have already observed that many cases of upper-level fronts in the literature are

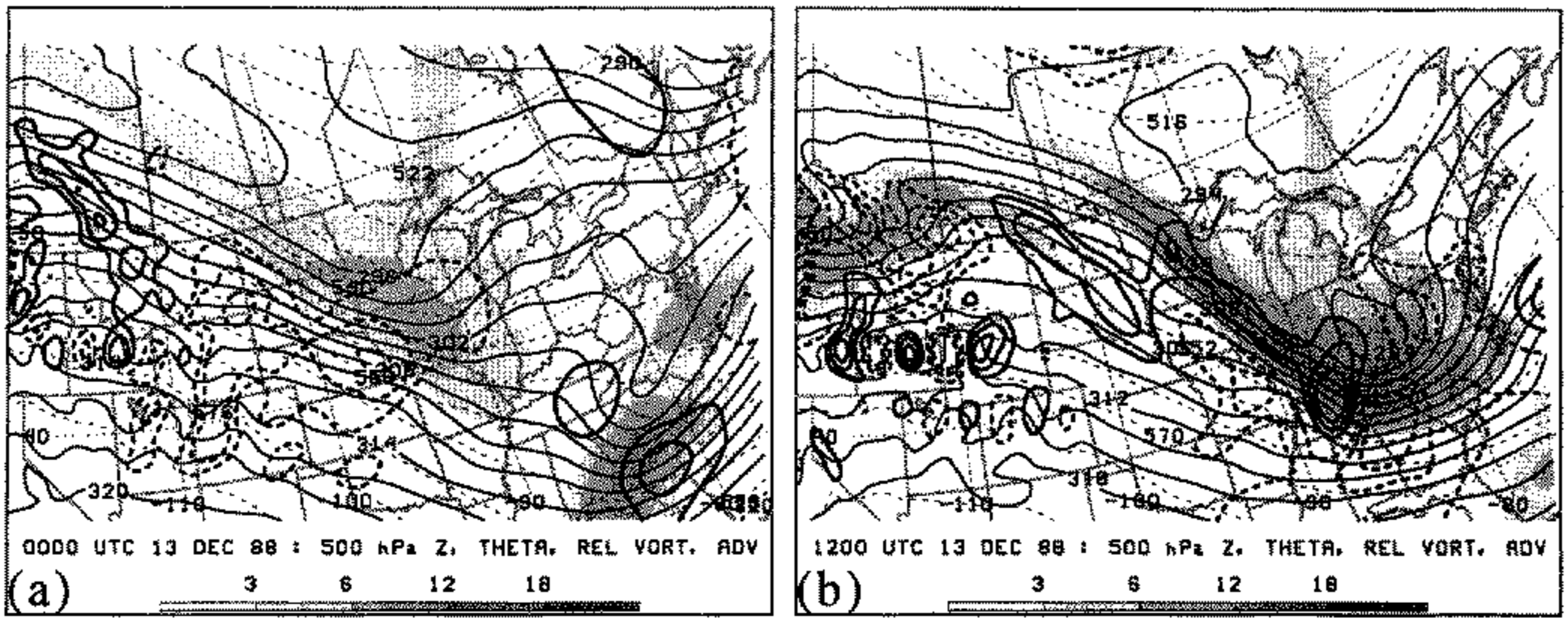

Figure 5. As in Fig. 3 except for NW (see text): (a) 0000 UTC 13 December 1988; (b) 1200 UTC 13 December 1988.

similar to NW. Therefore, we believe our results based on these two cases to be of some generality.

(c) *Vector-frontogenesis diagnostics*

In this section, we further examine SW and NW using the vector-frontogenesis diagnostics derived in section 2. In order to illustrate the behaviour of the vertical tilting terms in **F**, we present the 500 hPa vertical velocity. At 12/12, the vertical velocity for SW was characterized by descent on the west side of the trough and ascent on the east side of the trough, maximized within the region of strong potential-temperature gradient (Fig. 6(a)). This suggests, therefore, that the front was in a region of south-westerly flow unfavourable for further intensification by tilting. Note that the 'four-cell' pattern of ascent and descent associated with straight jet–front systems is masked by the vertical motions associated with the curvature of the flow (Uccellini (1990, section 6.3.1) and references therein). By 13/00, the pattern remained much the same (Fig. 6(b)). In contrast, descent was occurring on the warm side of the frontal zone in NW at 13/00 and 13/12 (Figs. 7(a) and (b)), favouring frontogenesis by tilting.

This hypothesis is confirmed by examining 500 hPa $-F_n$ and its components (divergence, deformation, and vertical-tilting) for SW and NW.* At 12/12 for SW, the divergence term was consistently smaller than the deformation term, which was positive along much of the front (cf. Figs. 8(a) and (b)). Figure 8(c) supports the interpretation from Fig. 6(a) that the ascent along the front was unfavourable for frontogenesis through tilting, as negative tilting frontogenesis occurred along the length of the front. As a result, the total scalar frontogenesis was positive along much of the length of the front, primarily supported by deformation (Figs. 8(b) and (d)). At 13/00, the divergence term was once again small compared to the deformation term (cf. Figs. 9(a) and (b)). Tilting resulted in frontolysis along the front so that the total frontogenesis was primarily a result of the deformation term (Figs. 9(b), (c) and (d)), a result consistent with other cases of upper-level frontogenesis in south-westerly flow (e.g. Bosart 1970).

The situation was quite different for NW. At 13/00, the divergence term was smaller than the deformation term, and both were negative along the equatorward side of the front (Figs. 10(a) and (b)). Tilting, on the other hand, was positive along

* We present $-F_n$ rather than F_n in order that regions of positive $-F_n$ represent regions of positive frontogenesis, according to (5a).

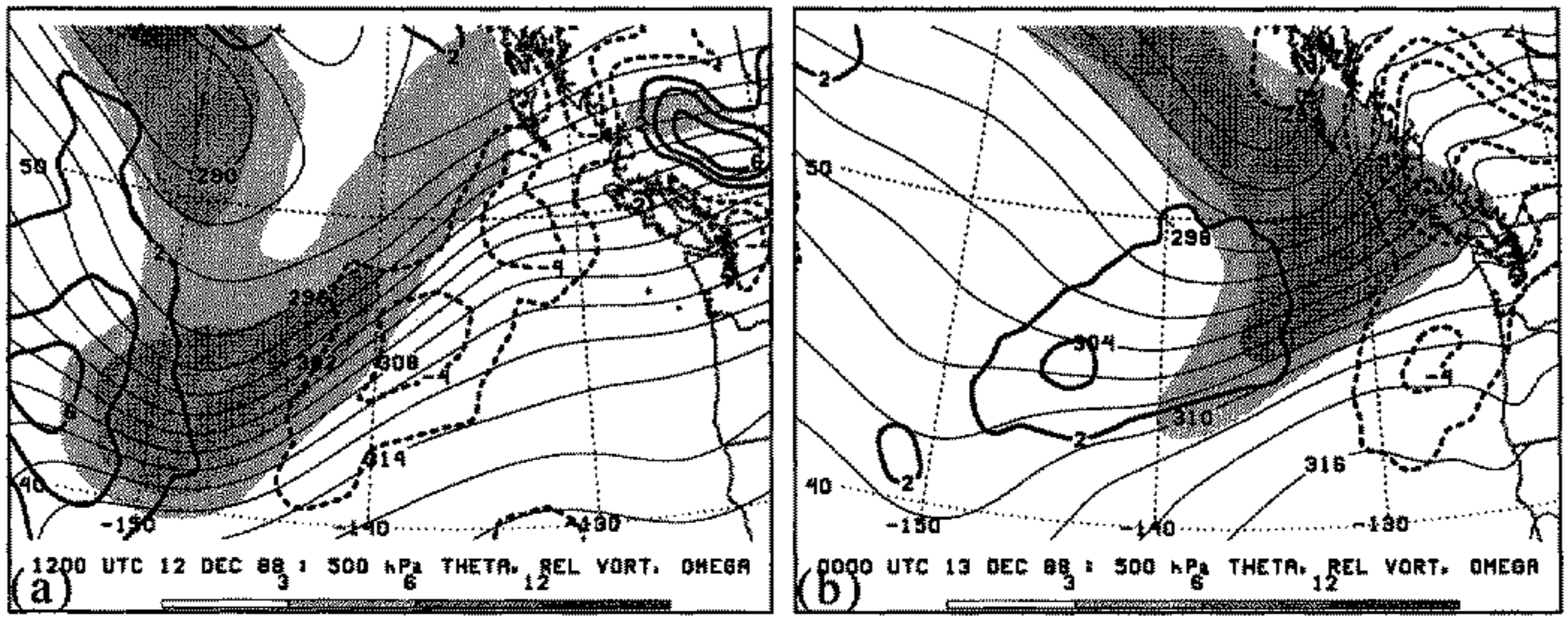

Figure 6. SW (see text) 500 hPa omega (pressure vertical velocity) (thick lines every 2 μb s^{-1}, from -8 to 8 μb s^{-1}; dashed (solid) lines represent ascent (descent)), potential temperature (thin solid lines every 2 K), and relative vorticity of total horizontal wind (10^{-5} s^{-1}, shaded according to scale at bottom of figure): (a) 1200 UTC 12 December 1988; (b) 0000 UTC 13 December 1988.

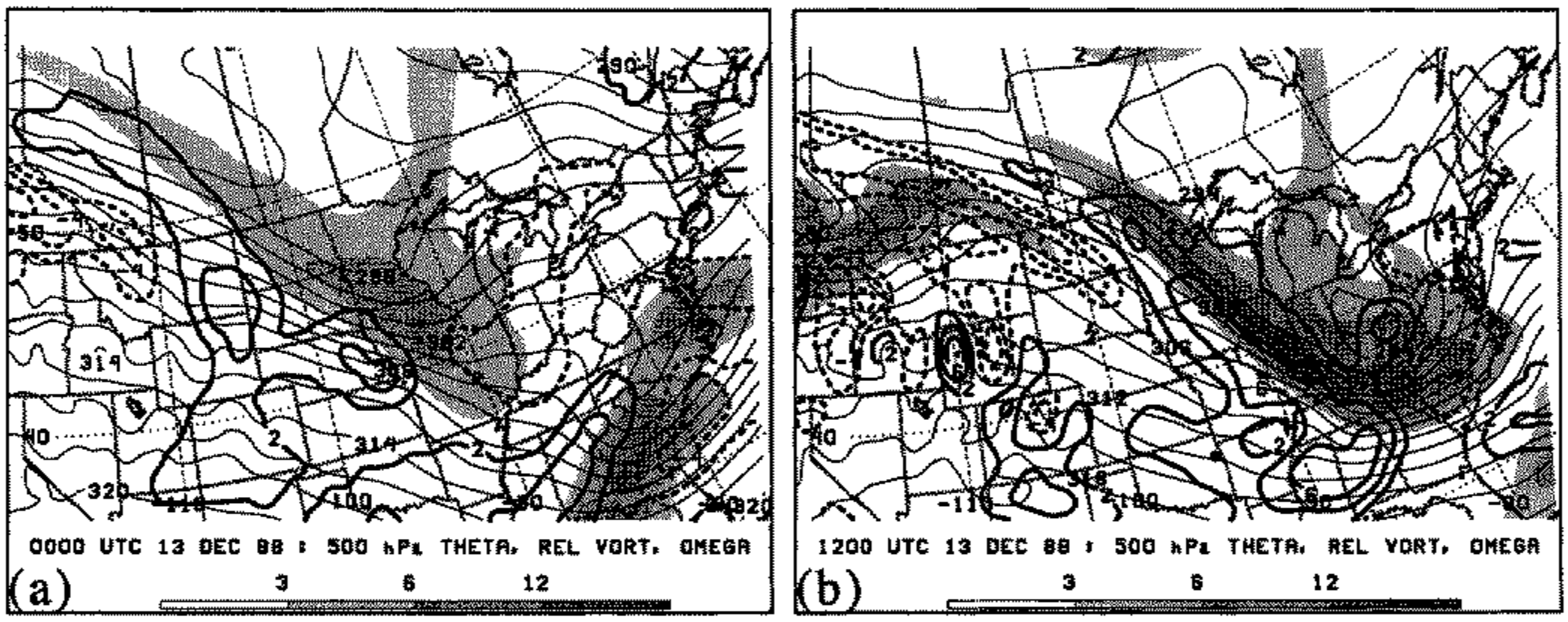

Figure 7. As in Fig. 6 except for NW (see text): (a) 0000 UTC 13 December 1988; (b) 1200 UTC 13 December 1988.

much of the front, and dominant along the north-west extent of the front (Figs. 10(c) and (d)) in the region of active frontogenesis. This confirms our hypothesis from Fig. 7(a) and the conclusion of Lackmann *et al.* (1997) that descent along the front results in frontogenesis through tilting. At 13/12, divergent and deformation frontolysis dominated along the poleward side of the front, maximized in the base of the thermal trough and along the north-west extent of the front (Figs. 11(a) and (b)). Even though tilting frontogenesis was positive along the length of the front, it was not large enough to offset the negative deformation frontogenesis, with the result that the total scalar frontogenesis was negative, maximized at the base of the thermal trough (Figs. 11(c) and (d)).

That the tilting frontogenesis for NW was maximum upstream of the strongest cold advection in a region of warm advection, particularly at 13/12, was noted in an earlier similar case study by Sanders *et al.* (1991, pp. 1339, 1364 and 1365). For SW, despite the presence of cold advection and confluence, frontogenetical tilting along the upper-level front did not occur (i.e. the Shapiro effect did not seem to be operating in SW). Uccellini

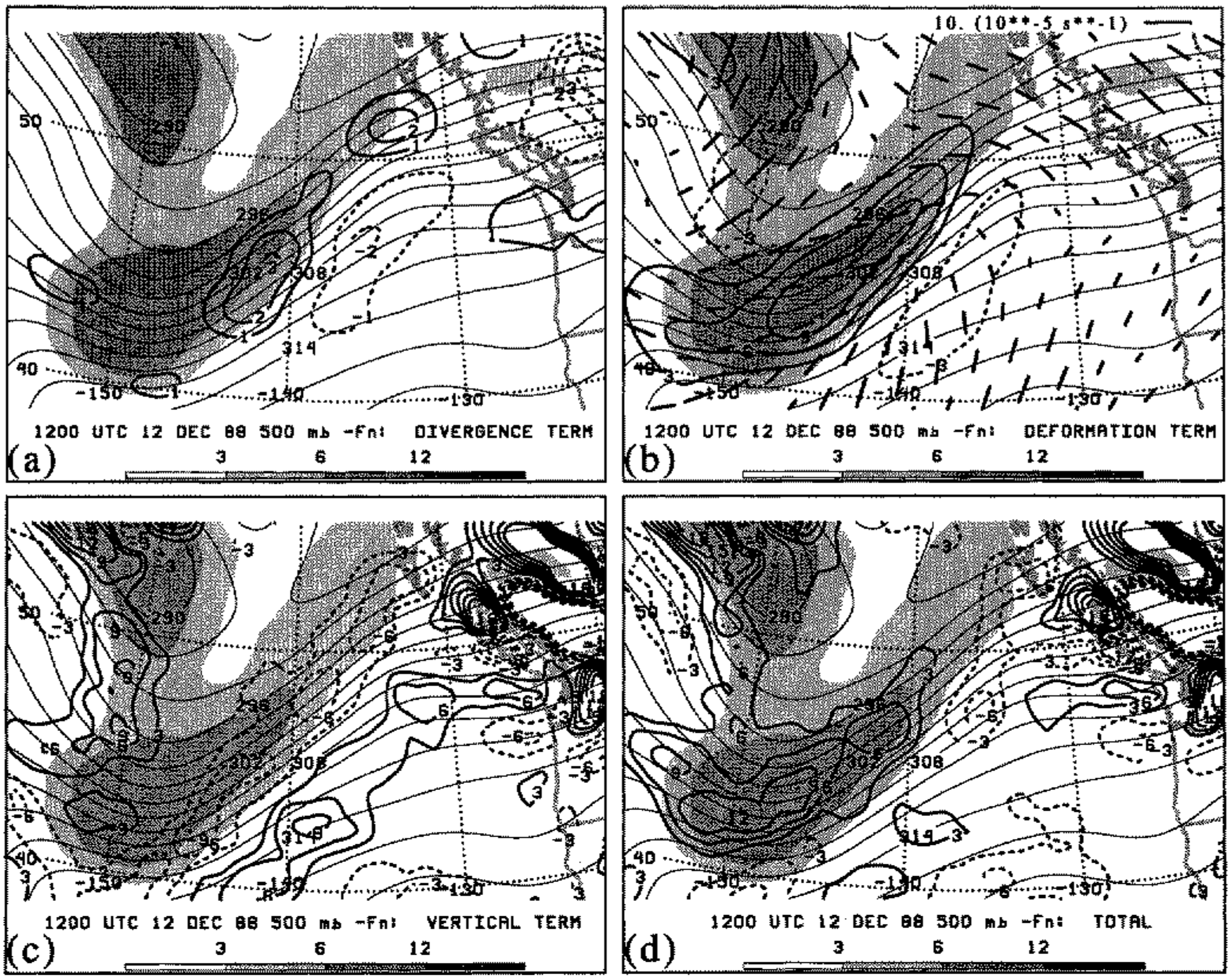

Figure 8. SW (see text) 500 hPa relative vorticity of total horizontal wind (10^{-5} s^{-1}, shaded according to scale at bottom of figure), and potential temperature (thin solid lines every 2 K) at 1200 UTC 12 December 1988: (a) $-F_n$ divergence term (every 1×10^{-10} K m^{-1} s^{-1}, from -6 to 6×10^{-10} K m^{-1} s^{-1}); (b) $-F_n$ deformation term (every 3×10^{-10} K m^{-1} s^{-1}, from -18 to 18×10^{-10} K m^{-1} s^{-1}) and axes of dilatation of total horizontal wind (10^{-5} s^{-1}, scaled according to legend; separation between displayed axes of dilatation is 180 km (every other grid point)); (c) $-F_n$ vertical tilting term (every 3×10^{-10} K m^{-1} s^{-1}, from -18 to 18×10^{-10} K m^{-1} s^{-1}); (d) total $-F_n$ (every 3×10^{-10} K m^{-1} s^{-1}, from -18 to 18×10^{-10} K m^{-1} s^{-1}).

et al. (1985, p. 978) and Pyle (1997, section 7.1) emphasized the importance of along-flow contributions to the vertical circulations around upper-level jet–front systems. This research, therefore, underscores the point made by these previous authors that two-dimensional conceptualizations of jet–front circulations can be difficult to apply to the real atmosphere in regions of curved flow.

We next examine 500 hPa F_s and its components for SW and NW. At 12/12 for SW, the vorticity term in F_s was largest along the vorticity maximum, with the deformation term negative along the north-eastern extent of the front (Figs. 12(a) and (b)). Positive F_s implies cyclonic rotation of the isentropes, consistent with positive vorticity in that area. Tilting led to negative F_s, anticyclonic rotation of the isentropes, which favoured eastward migration of the thermal trough (Fig. 12(c)). Total F_s was a maximum in the base of the thermal trough (Fig. 12(d)), due primarily to the vorticity term (Fig. 12(a)). It was this feature that resulted in the cyclonic rotation of the isentropes relative to the flow field, thereby initiating cold advection along the front in the base of the thermal trough (see footnote on p. 13). At 13/00 after the onset of cold advection, patterns similar to that at 12/12 existed along the front. The dominant term was the vorticity term, maximum

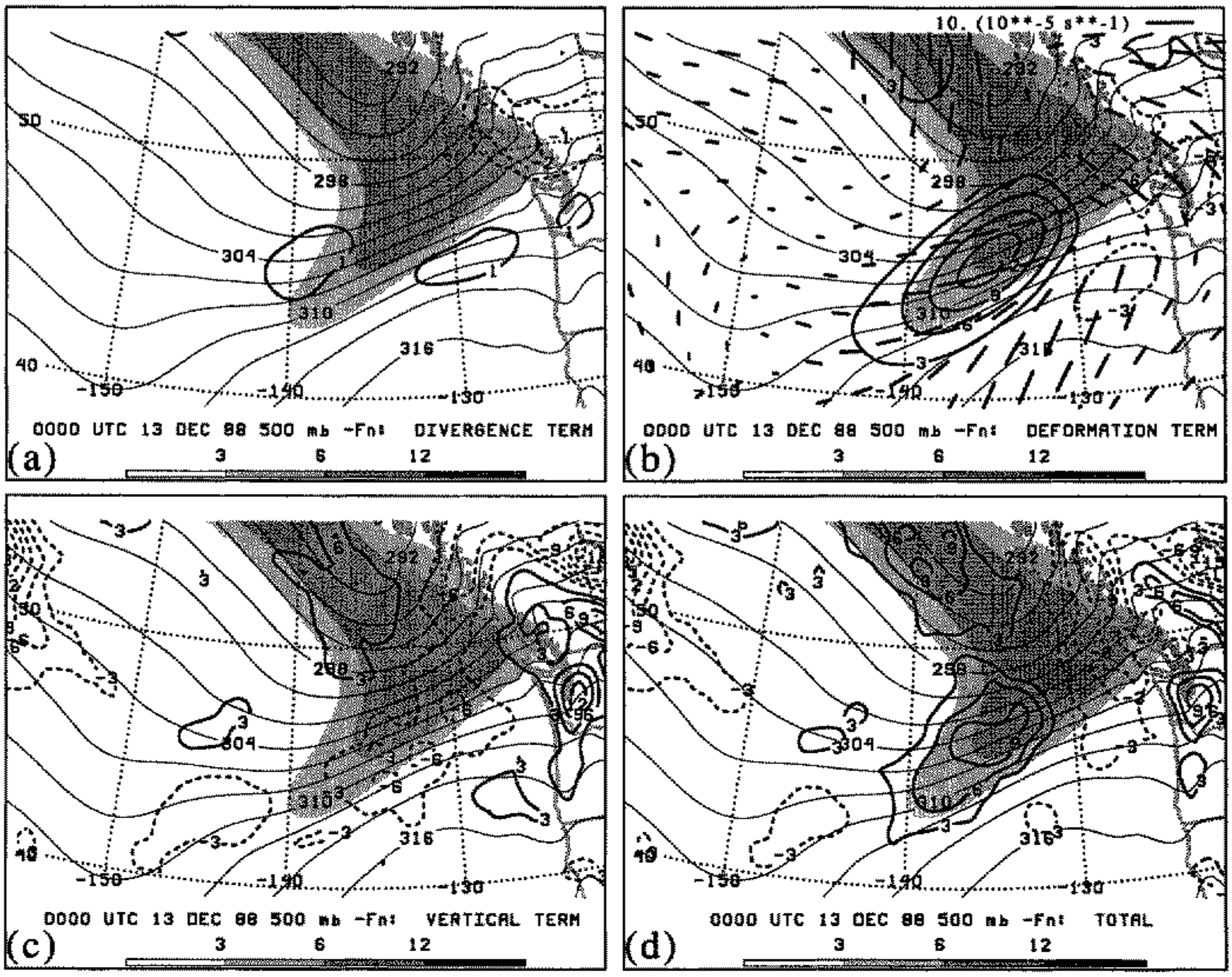

Figure 9. As in Fig. 8 except for 0000 UTC 13 December 1988.

along the length of the front (Figs. 13(a) and (d)). The deformation and vertical terms were smaller and negative (Figs. 13(b) and (c)). Total F_s was thus positive along most of the length of the front (Fig. 13(d)), consistent with the cyclonic rotation of the isentropes leading to cold advection along the length of the front.

For NW at 13/00, the vorticity term was positive along the front (Fig. 14(a)) and the deformation term was negative along the upstream part of the front (Fig. 14(b)), as opposed to the downstream part of the front in SW (Fig. 12(b)). With the negative contribution from the vertical term (Fig. 14(c)), the total F_s was positive at the leading downstream edge of the front (Fig. 14(d)), thereby implying that the rotation of isentropes leading to cold advection occurred here, as opposed to the upstream edge of the front in SW. This pattern was repeated and intensified at 13/12 (Fig. 15). The vorticity term dominated (Fig. 15(a)), but was offset by the deformation term along the northwest extension of the front upstream (Fig. 15(b)). Tilting was weak or negative such that the total F_s implied cyclonic rotation of the isentropes occurring in the base of the thermal trough (Figs. 15(c) and (d)), in agreement with the region of cold advection in Fig. 5(b).

To examine these results further, we employed the methodology of Keyser *et al.* (1989) and Loughe *et al.* (1995) to calculate the divergent and rotational wind explicitly. Calculations of vector frontogenesis using these wind components (not shown) illustrate that the 500 hPa rotational wind was primarily responsible for the 500 hPa rotational frontogenesis, resulting in the transition to cold advection along the front. Also, the

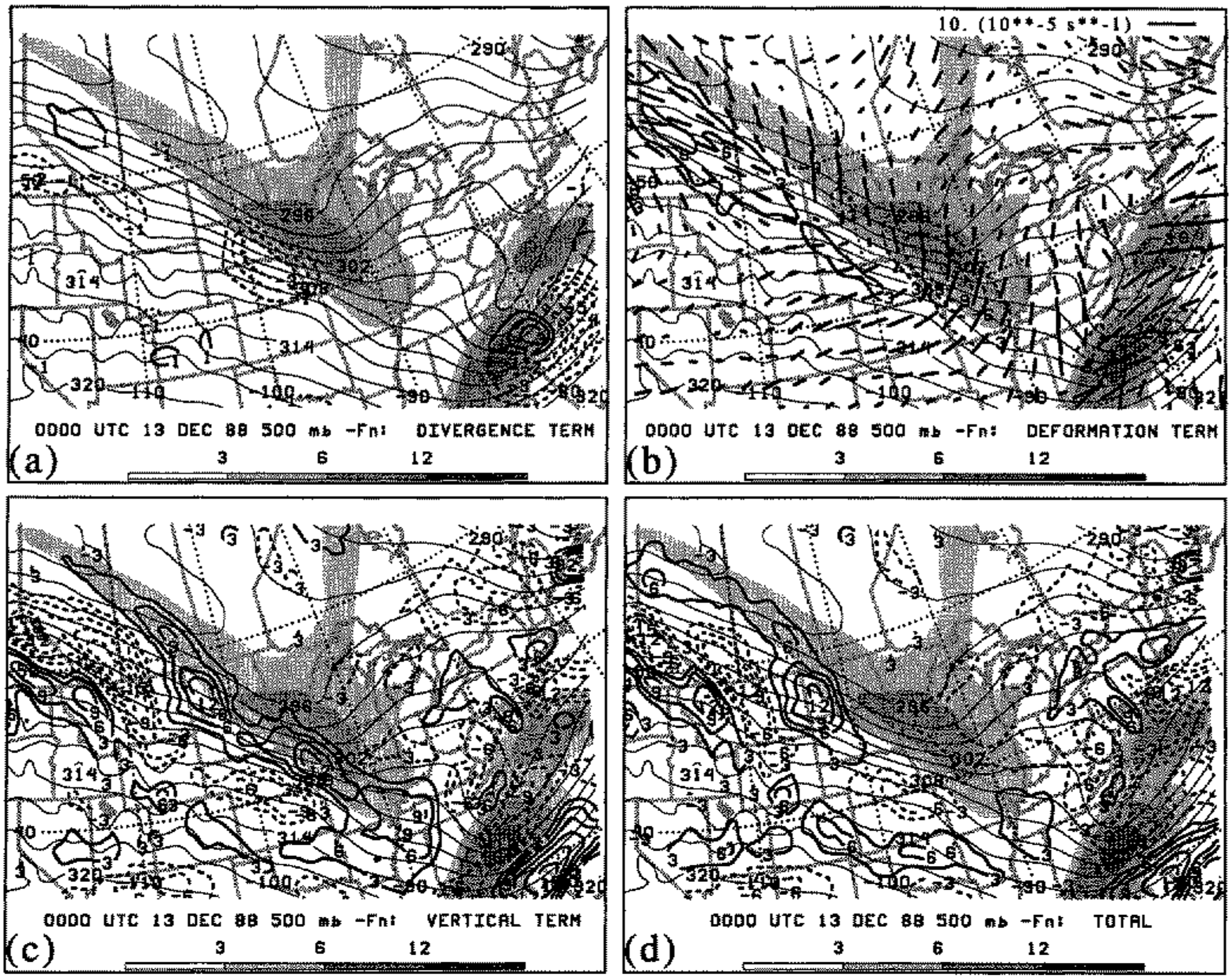

Figure 10. As in Fig. 8 except for NW (see text) at 0000 UTC 13 December 1988.

contribution of the divergent wind field to frontogenesis at 500 hPa is small. This confirms our earlier results using the vector-frontogenesis diagnostics on the total wind field.

4. Climatology of upper-level fronts over the eastern North Pacific Ocean

In order to assess the frequency of occurrence of the evolution epitomized by SW, a climatology of upper-level fronts associated with landfalling North Pacific surface cyclones was compiled. The NMC *Daily Weather Map* series was examined for all cases of North Pacific surface cyclones crossing the western coast of North America between 35°N and 60°N in December, January, and February (DJF) for the six winters 1988–89 through 1993–94. The NMC 500 hPa analyses associated with each cyclone were then characterized according to two different subjective criteria. First, the 500 hPa flow was identified as south-westerly, north-westerly, zonal, or other (e.g. closed low). Second, the thermal evolution of the 500 hPa baroclinicity was then classified as equivalent-barotropic stage to cold-advection stage (i.e. increasing cold advection), decreasing cold advection, weak advection or equivalent-barotropic stage, warm advection, or a combination of the above. The results from this climatology are presented in Table 2.

Of the 19–30 winter (DJF) cyclones per year that made landfall on the west coast of North America during the six-year period of our climatology, 44% occurred in south-westerly flow versus 14% in north-westerly flow (Table 2), consistent with the wintertime-averaged south-westerly jet stream over the eastern North Pacific Ocean (e.g.

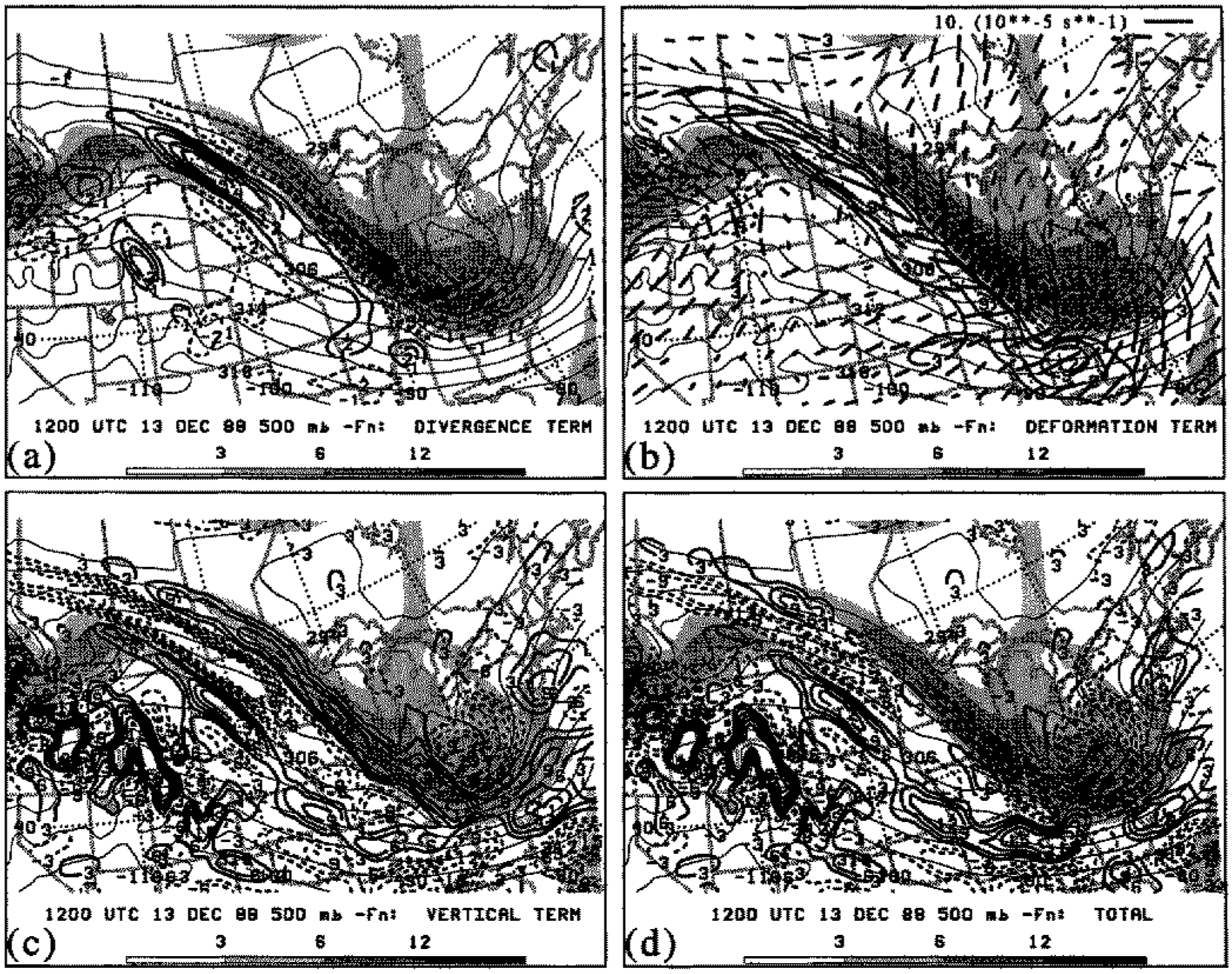

Figure 11. As in Fig. 8 except for NW (see text) at 1200 UTC 13 December 1988.

TABLE 2. CLIMATOLOGY OF UPPER-LEVEL FRONTS (SEE TEXT FOR FURTHER DETAILS)

Category	Six-year total	Yearly range	Percent of total
Number of cyclones	149	19–30	100
South-westerly flow	66	6–16	44
North-westerly flow	21	1–6	14
Zonal flow	18	0–6	12
Other flow	44	3–14	30
Equivalent barotropic to cold advection	35	1–10	23
Decreasing cold advection	19	0–6	13
Weak advection or equivalent barotropic	73	7–21	49
Warm advection	5	0–2	3
Combination	17	1–6	11

Percentages may not add up to 100% due to round-off of decimal values.

Sanders 1988, Fig. 7; Bluestein 1993, Fig. 1.72(a); Lackmann *et al.* 1996, Fig. 1). With regard to the thermal evolution of the baroclinic zone, the largest percentage (49%) was characterized by weak thermal advection, indicating relatively old, nearly equivalent-barotropic systems, characteristic of cyclones at the end of their evolutions over the eastern North Pacific Ocean. The second largest group (23%) comprised those events that underwent the change from equivalent barotropic to cold advection.

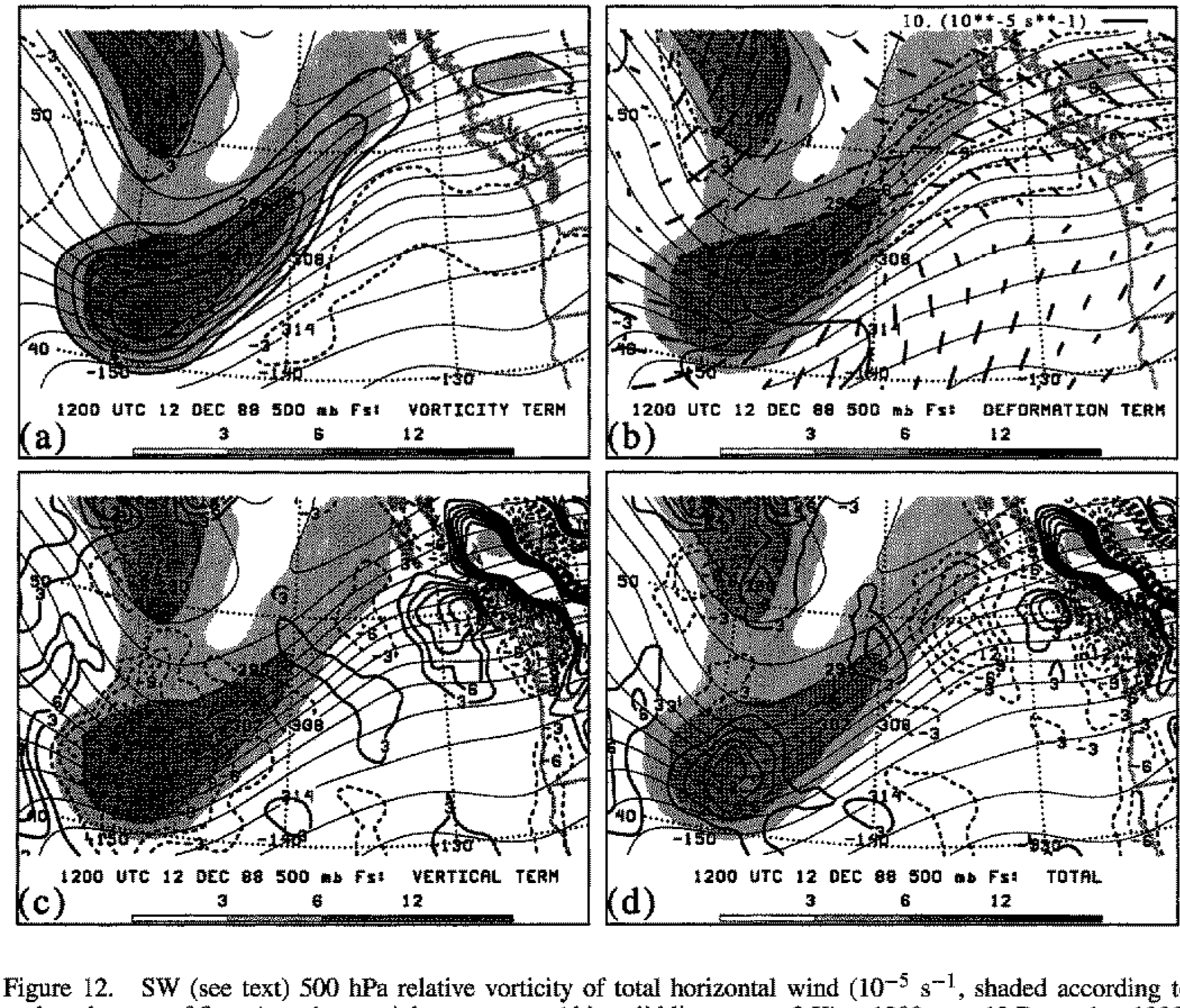

Figure 12. SW (see text) 500 hPa relative vorticity of total horizontal wind (10^{-5} s^{-1}, shaded according to scale at bottom of figure), and potential temperature (thin solid lines every 2 K) at 1200 UTC 12 December 1988: (a) F_s vorticity term (every 3×10^{-10} K m^{-1} s^{-1}, from -18 to 18×10^{-10} K m^{-1} s^{-1}); (b) F_s deformation term (every 3×10^{-10} K m^{-1} s^{-1}, from -18 to 18×10^{-10} K m^{-1} s^{-1}) and axes of dilatation of total horizontal wind (10^{-5} s^{-1}, scaled according to legend; separation between displayed axes of dilatation is 180 km (every other grid point)); (c) F_s vertical tilting term (every 3×10^{-10} K m^{-1} s^{-1}, from -18 to 18×10^{-10} K m^{-1} s^{-1}); (d) total F_s (every 3×10^{-10} K m^{-1} s^{-1}, from -18 to 18×10^{-10} K m^{-1} s^{-1}).

Those 23% (35 events in total) that evolved from a state of equivalent barotropy to a state of cold advection were then examined separately (Table 3). Of these 35 events, 63% occurred in south-westerly flow, or 15% of the total of 149 cyclones. Of the 66 events that occurred in south-westerly flow (Table 2), 33% (22/66) evolved from equivalent barotropy to cold advection (not shown). This is in comparison to the 29% (6/21) of the north-westerly flow cases and the 28% (5/18) of the zonal-flow cases that underwent this evolution (not shown). Since the evolution from equivalent barotropic to cold advection occurs at roughly the same rate regardless of flow type, it seems that the predominance of south-westerly flow fronts that evolve from equivalent barotropic to cold advection is favoured in this area owing to the climatological tendency for south-westerly flow, rather than some inherent tendency for cold advection to develop from an initial state of equivalent barotropy, preferentially, in south-westerly versus north-westerly or zonal flow. Results from Tables 2 and 3 indicate, therefore, that the SW evolution displayed in Fig. 3, although not the only upper-level frontal evolution possible in south-westerly flow, is relatively common on the west coast of North America.

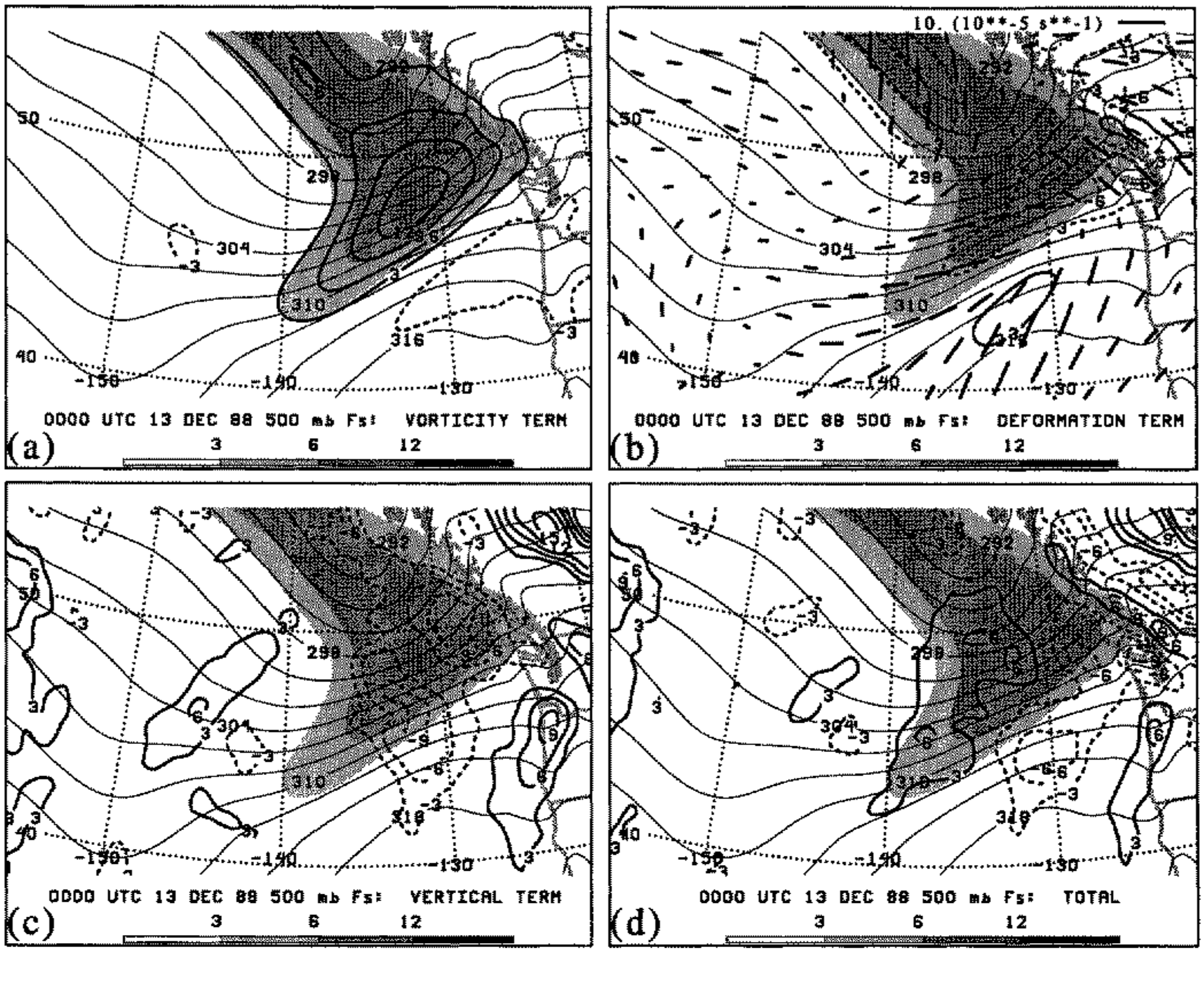

Figure 13. As in Fig. 12 except for 0000 UTC 13 December 1988.

TABLE 3. CLIMATOLOGY OF EQUIVALENT-BAROTROPIC STAGE TO COLD-ADVECTION STAGE EVENTS FROM TABLE 2

Category	Six-year total	Yearly range	Percent of total
Number of cyclones:			
Equivalent barotropic to cold advection	35	1–10	100
South-westerly flow	22	1–8	63
North-westerly flow	6	0–3	17
Zonal flow	5	0–2	14
Other flow	2	0–1	6

It should be noted that this evolution in south-westerly flow from nearly equivalent barotropic to cold advection is not necessarily limited to over the eastern North Pacific Ocean. We would expect similar evolutions to SW to be common in regions where relatively old, nearly equivalent-barotropic systems traverse regions of climatological south-westerly flow (e.g. the eastern North Atlantic Ocean). Indeed, similar evolutions elsewhere have been documented in the literature: Bjerknes (1951, Figs. 11, 12, and 14), McGinnigle *et al.* (1988, Fig. 7), and Cammas and Ramond (1989, their case JS2, Figs. 2(a) and 19).

Additionally, Sinclair (1998, personal communication), has performed composite analyses of cyclogenesis in different large-scale flows over the western South Pacific Ocean. For a composite of cyclones that develop in the equatorward entrance region

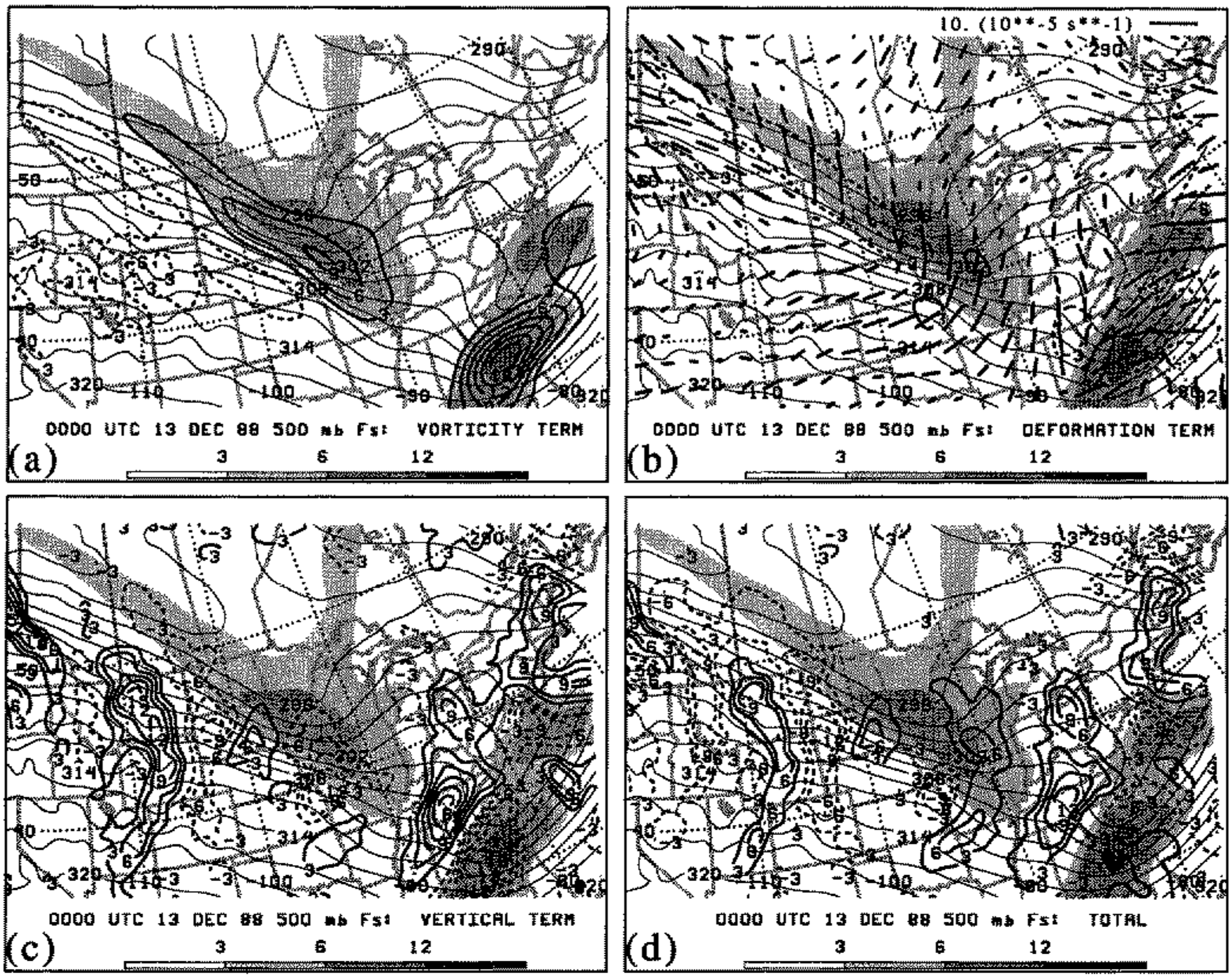

Figure 14. As in Fig. 12 except for NW (see text) at 0000 UTC 13 December 1988.

of an upper-level jet streak (his classification E; Sinclair and Revell (1999, personal communication)), the 500 hPa thermal evolution resembles that of SW, whereas for a composite of cyclones that develop in the diffluent exit region of an upstream upper-level jet streak (his classification U; Sinclair and Revell (1999, personal communication)), the 500 hPa thermal evolution resembles that of NW. These results are consistent with those presented in this paper.

5. Concluding discussion

We have presented the structure and early evolution of two case studies of upper-level frontogenesis. As discussed in sections 1(a) and 4, we believe these cases are reasonably representative of many upper-level fronts. The Shapiro conceptual model suggests that the evolution from equivalent barotropic to cold advection along the length of the front occurs in north-westerly flow. We found that this schematic evolution more closely resembles that which may occur in south-westerly flow instead. North-westerly flow fronts, however, tend to concentrate the cold advection in the base of the thermal trough, in contrast with the Shapiro conceptual model.

(*a*) *Revised conceptual model*

Therefore, the results of this research lead us to revise the Shapiro conceptual model. Figure 16(a) presents the schematic evolution of an upper-level front in south-westerly

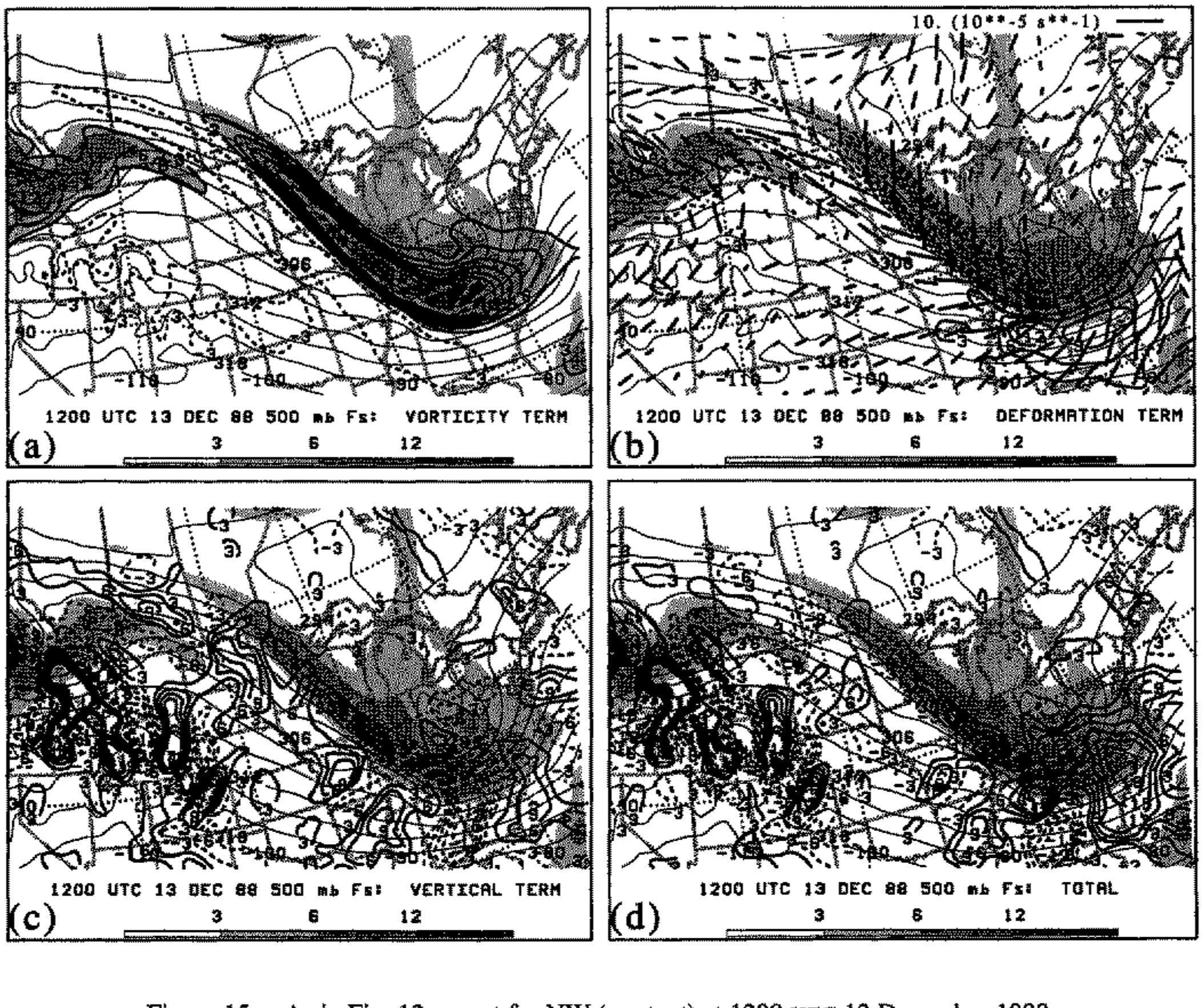

Figure 15. As in Fig. 12 except for NW (see text) at 1200 UTC 13 December 1988.

flow over the eastern North Pacific Ocean. Initially, the isotherms and the isohypses are relatively parallel. The advance of an upstream vorticity maximum towards the baroclinic zone leads to the rotation of the isentropes relative to the height contours, resulting in the onset of cold advection. This revised model differs from the original Shapiro conceptual model because this evolution occurs in south-westerly, rather than north-westerly, flow and the vorticity maximum is shown to be responsible for the onset of the cold advection.

In contrast, Fig. 16(b) presents the schematic evolution of an upper-level front in north-westerly flow over North America. Initial cold advection along the length of the front becomes concentrated in the base of the thermal trough in conjunction with an intensifying and compacting vorticity maximum in north-westerly flow. Upstream of the thermal trough, warm advection is typically occurring in the north-westerly flow, indicating substantial along-front variation in thermal advection, in contrast with the Shapiro conceptual model.

(*b*) *Thermal advection along upper-level fronts*

During the evolution from equivalent barotropy to cold advection in SW, the rotation of the isentropes relative to the height field was initiated by the approach of an upstream vorticity maximum towards the baroclinic zone. As illustrated by the F_s diagnostics, the rotation was attributed to the vorticity contribution to F_s, the vertical and deformation terms being negative or small. Similar rotation of the isentropes was also observed

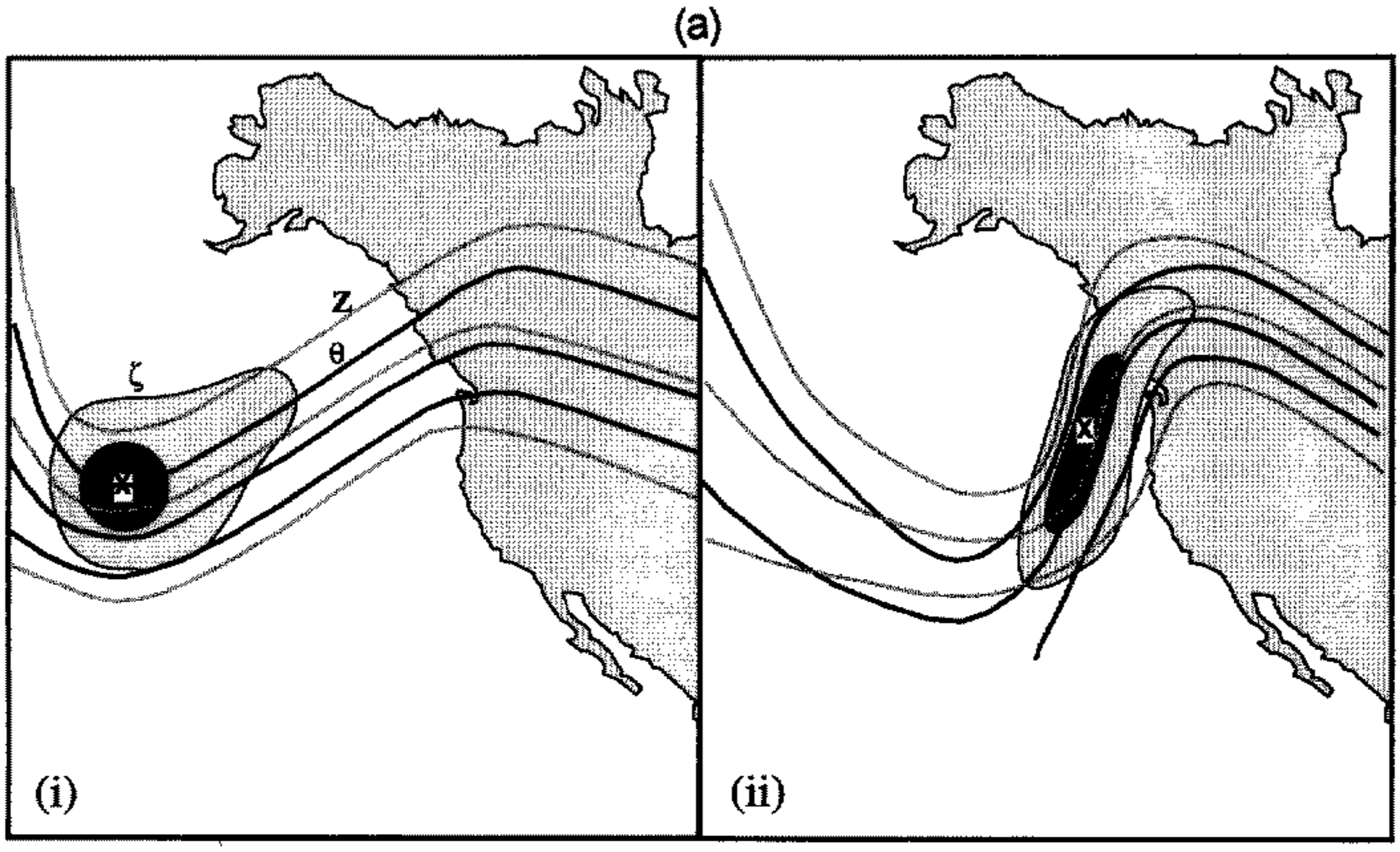

Figure 16. Revised conceptual model: Idealized schematic depiction, on an upper-tropospheric isobaric surface, of the early evolution of an upper-level jet–front system through a mid-latitude baroclinic wave over a 12–24 h period: (a) south-westerly flow case; (b) north-westerly flow case. Geopotential height contours (solid grey lines) and labelled Z in (a)(i), isentropes (solid black lines) are labelled θ in (a)(i), and relative vorticity (shaded) is labelled ζ in (a)(i).

in NW near the base of the thermal trough. Once the rotation of the isentropes by the approaching vorticity maximum is accomplished and thermal advection becomes significant, the dynamical processes associated with that advection are likely to become significant also. Therefore, it appears that vector frontogenesis is useful in a variety of large-scale flow regimes to identify when this change in structure will occur and provides operational forecasters with a methodology to forecast this transition.

A mechanism for the onset of cold advection along upper-level fronts was suggested previously by Rotunno *et al.* (1994, pp. 3390 and 3391) and discussed further in Keyser (1999, personal communication). Based on their analysis of normal-mode cyclogenesis in a baroclinic primitive-equation channel model, Rotunno *et al.* (1994) hypothesized that the transition to along-front cold advection in the confluent jet-entrance region (the Shapiro effect) was due to the subsidence along the upper-level front bringing down higher potential-temperature air from aloft, thereby implying a horizontal rotation of the isentropes. This mechanism would appear to implicate the vertical tilting term in F_s, s_3 in (11b), in contrast with our results that implicate the vorticity term in F_s in both SW and NW. In fact, the tilting term in both SW and NW acted in the opposite direction (anticylonic rotation of the isentropes) than that which was observed to occur (cyclonic rotation of the isentropes) (Figs. 12(c), 13(c), 14(c), and 15(c)). It may be that this apparent discrepancy is a result of the tilting process being important at the earliest stages of upper-level frontogenesis, whereas the rotation becomes important later, at the time of our analyses. The relative importance of different processes on frontogenesis at different times during the evolution of upper-level fronts, however, is a subject of continuing research.

We also note that the evolution shown in Rotunno *et al.* (1994) more closely resembles NW than SW, a point made previously by Lackmann *et al.* (1997, pp. 2755 and 2756). Whereas the tilting of vorticity greatly intensified a weak vorticity maximum in NW, SW possessed a pre-existing vorticity maximum that did not change intensity substantially. Idealized normal-mode model experiments by their nature must generate vorticity maxima from a basic state with very small initial disturbances. This comparison has already been noted by Keyser and Shapiro (1986, p. 494), who state, 'Although realistic reproductions of upper-level and surface fronts are found in the context of baroclinic instability theory, they arise as a consequence of upper-level wave amplification and low-level cyclogenesis, rather than appearing in advance of these processes'. As we have shown here, the evolution of upper-level fronts is intimately related to vorticity maxima pre-existing (SW) or developing concomitantly with the upper-level front (NW). The large-scale flow, therefore, acts to position the upper-level fronts and the vorticity maxima into an appropriate configuration.

(*c*) *Future research*

An extension of this study would be to perform a climatology, as in section 4, except for events occurring over north-central North America, the region characterized in the Shapiro conceptual model and where previous studies indicate frequent north-westerly flow frontogenesis (Sanders 1988; Lackmann *et al.* 1996). Another topic of interest is the later evolution of the cases presented in this paper. The later evolution of NW has been documented by Lackmann *et al.* (1997) and Hakim (1997). For SW, the eventual movement of that front over the intermountain region of the western United States and subsequent reintensification in the lee of the Rockies was complicated by the existence of the mountains.

ACKNOWLEDGEMENTS

We are deeply indebted to the following individuals for their contributions to this work: Prof. Jim Steenburgh and Dr David Stensrud for their assistance using MM5; Prof. Steenburgh and Matt Pyle for discussions on upper-level frontogenesis; and Prof. Daniel Keyser, Dr Rich Rotunno, Prof. Gary Lackmann, Matt Wandishin, Dr John Cortinas, Dr Greg Hakim, Dr Mel Shapiro, Dr Conrad Ziegler, and an anonymous reviewer for their comments on an earlier version of this manuscript. Dr Mark Sinclair graciously performed composite analyses of his cyclone dataset at our request. Dr Hakim suggested the analysis using the Loughe *et al.* (1995) methodology, Dr David Knight provided the source code, and Matt Pyle assisted with its implementation. The satellite imagery presented in Fig. 4 was obtained courtesy of the National Environmental Satellite Data and Information Service and the National Climatic Data Center. Access to the Storm Prediction Center's archived weather maps on microfilm is gratefully acknowledged. We are grateful to the Data Support Section of the Scientific Computing Division of NCAR for providing data used in this study, and the Mesoscale and Microscale Meteorology Division of NCAR for their support of MM5.

This research was conducted while the first author was a National Research Council postdoctoral research associate at the National Severe Storms Laboratory.

REFERENCES

Bader, M. J., Forbes, G. S., Grant, J. R., Lilley, R. B. E. and Waters, A. J. 1995 *Images in weather forecasting*. Cambridge University Press, UK

Bell, G. D. and Bosart, L. F. 1994 Midtropospheric closed cyclone formation over the south-western United States, the eastern United States, and the Alps. *Mon. Weather Rev.*, **122,** 791–813

Bell, G. D. and Keyser, D. 1993 Shear and curvature vorticity and potential-vorticity interchanges: Interpretation and application to a cutoff cyclone event. *Mon. Weather Rev.*, **121,** 76–102

Benjamin, S. G. and Seaman, N. L. 1985 A simple scheme for objective analysis in curved flow. *Mon. Weather Rev.*, **113,** 1184–1198

Berggren, R. 1952 The distribution of temperature and wind connected with active tropical air in the higher troposphere and some remarks concerning clear air turbulence at high altitude. *Tellus*, **4,** 43–53

Bjerknes, J. 1951 Extratropical cyclones. Pp. 577–598 in *Compendium of meteorology*. Ed. T. F. Malone. American Meteorological Society, Boston, USA

Bjerknes, J. and Palmén, E. 1937 Investigations of selected European cyclones by means of serial ascents. *Geophys. Publ.*, **12**(2), 1–62

Bluestein, H. B. 1986 Fronts and jet streaks: A theoretical perspective. Pp. 173–215 in *Mesoscale meteorology and forecasting*. Ed. P. S. Ray. American Meteorological Society, Boston, USA

1993 *Synoptic-dynamic meteorology in midlatitudes. Volume II: Observations and theory of weather systems*. Oxford University Press, UK

Bosart, L. F. 1970 Mid-tropospheric frontogenesis. *Q. J. R. Meteorol. Soc.*, **96,** 442–471

Cammas, J.-P. and Ramond, D. 1989 Analysis and diagnosis of the composition of ageostrophic circulations in jet–front systems. *Mon. Weather Rev.*, **117,** 2447–2462

Carlson, T. N. 1991 *Mid-latitude weather systems*. Harper Collins, New York, USA

Cunningham, P. and Keyser, D. 1996 'Numerical modelling of jet-streak dynamics'. Pp. 20–22 in Preprints, Seventh Conference on Mesoscale Processes, 9–13 September 1996, Reading, United Kingdom. American Meteorological Society, Boston, USA

Danielsen, E. F. 1964 'Project Springfield report'. DASA 1517. Defense Atomic Support Agency

Djurić, D. 1994 *Weather analysis*. Prentice-Hall Inc., Englewood Cliffs, USA

Dudhia, J. 1989 Numerical study of convection observed during the Winter Monsoon Experiment using a mesoscale two-dimensional model. *J. Atmos. Sci.*, **46,** 3077–3107

1993 A nonhydrostatic version of the Penn State–NCAR mesoscale model: Validation tests and simulation of an Atlantic cyclone and cold front. *Mon. Weather Rev.*, **121,** 1493–1513

Evans, M. S., Keyser, D., Bosart, L. F. and Lackmann, G. M. 1994 A satellite-derived classification scheme for rapid maritime cyclogenesis. *Mon. Weather Rev.*, **122,** 1381–1416

Grell, G. A., Dudhia, J. and Stauffer, D. R. 1994 'A description of the fifth-generation Penn State/NCAR Mesoscale Model (MM5)'. NCAR Tech. Note NCAR/TN–398+STR, NCAR, P.O. Box 3000, Boulder, CO 80307-3000, USA

Hakim, G. J. 1997 'Extratropical cyclogenesis in terms of baroclinic vortex dynamics'. Ph.D. dissertation, University at Albany, State University of New York

Hines, K. M. and Mechoso, C. R. 1991 Frontogenesis processes in the middle and upper troposphere. *Mon. Weather Rev.*, **119,** 1225–1241

Kain, J. S. and Fritsch, J. M. 1993 Convective parameterization for mesoscale models: The Kain–Fritsch scheme. Pp. 165–170 in *The representation of cumulus convection in numerical models*. Meteor. Monogr., No. 24, American Meteorological Society, Boston, USA

Keyser, D. and Pecnick, M. J. 1985 A two-dimensional primitive equation model of frontogenesis forced by confluence and horizontal shear. *J. Atmos. Sci.*, **42,** 1259–1282

Keyser, D. and Shapiro, M. A. 1986 A review of the structure and dynamics of upper-level frontal zones. *Mon. Weather Rev.*, **114,** 452–499

Keyser, D., Pecnick, M. J. and Shapiro, M. A. 1986 Diagnosis of the role of vertical deformation in a two-dimensional primitive equation model of upper-level frontogenesis. *J. Atmos. Sci.*, **43,** 839–850

Keyser, D., Reeder, M. J. and Reed, R. J. 1988 A generalization of Petterssen's frontogenesis function and its relation to the forcing of vertical motion. *Mon. Weather Rev.*, **116,** 762–780

Keyser, D., Schmidt, B. D. and Duffy, D. G. 1989 A technique for representing three-dimensional vertical circulations in baroclinic disturbances. *Mon. Weather Rev.*, **117,** 2463–2494

Klemp, J. B. and Durran, D. R. 1983 An upper boundary condition permitting internal gravity wave radiation in numerical mesoscale models. *Mon. Weather Rev.*, **111,** 430–444

Krishnamurti, T. N. 1968 A study of a developing wave cyclone. *Mon. Weather Rev.*, **96,** 208–217

Lackmann, G. M., Bosart, L. F. and Keyser, D. 1996 Planetary-and synoptic-scale characteristics of explosive wintertime cyclogenesis over the western North Atlantic Ocean. *Mon. Weather Rev.*, **124,** 2672–2702

Lackmann, G. M., Keyser, D. and Bosart, L. F. 1997 A characteristic life cycle of upper-tropospheric cyclogenetic precursors during the Experiment on Rapidly Intensifying Cyclones over the Atlantic (ERICA). *Mon. Weather Rev.*, **125,** 2729–2758

Lalaurette, F., Fischer, C. and Cammas, J.-P. 1994 Location and interaction of upper- and lower-troposphere adiabatic frontogenesis. *Mon. Weather Rev.*, **122,** 2004–2021

Loughe, A. F., Lai, C.-C. and Keyser, D. 1995 A technique for diagnosing three-dimensional ageostrophic circulations in baroclinic disturbances on limited-area domains. *Mon. Weather Rev.*, **123,** 1476–1504

McGinnigle, J. B., Young, M. V. and Bader, M. J. 1988 The development of instant occlusions in the North Atlantic. *Meteorol. Mag.*, **117,** 325–341

Miller, J. E. 1948 On the concept of frontogenesis. *J. Meteorol.*, **5,** 169–171

Namias, J. and Clapp, P. F. 1949 Confluence theory of the high tropospheric jet stream. *J. Meteorol.*, **6,** 330–336

Neiman, P. J. and Shapiro, M. A. 1989 Retrieving horizontal temperature gradients and advections from single-station wind profiler observations. *Weather and Forecasting*, **4,** 222–233

Newton, C. W. 1954 Frontogenesis and frontolysis as a three-dimensional process. *J. Meteorol.*, **11,** 449–461

1958 Variations in frontal structure of upper level troughs. *Geophysica*, **6,** 357–375

Newton, C. W. 1965 Variations in structure of subtropical current system accompanying a deep polar outbreak. *Mon. Weather Rev.*, **93,** 101–110

Newton, C. W. and Carson, J. E. 1953 Structure of wind field and variations of vorticity in a summer situation. *Tellus*, **5,** 321–339

Newton, C. W. and Persson, A. V. 1962 Structural characteristics of the subtropical jet stream and certain lower-stratospheric wind systems. *Tellus*, **14,** 221–241

Newton, C. W. and Palmén, E. 1963 Kinematic and thermal properties of a large-amplitude wave in the westerlies. *Tellus*, **15,** 99–119

Orlanski, I. and Sheldon, J. P. 1995 Stages in the energetics of baroclinic systems. *Tellus*, **47A,** 605–628

Palmén, E. and Nagler, K. M. 1949 The formation and structure of a large-scale disturbance in the westerlies. *J. Meteorol.*, **6,** 227–242

Palmén, E. and Newton, C. W. 1969 *Atmospheric circulation systems*. Academic Press, Orlando, USA

Petterssen, S. 1936 Contribution to the theory of frontogenesis. *Geophys. Publ.*, **11**(6), 1–27

Pyle, M. E. 1997 'A diagnostic study of jet streaks: Kinematic signatures and relationship to coherent tropopause disturbances'. M.S. thesis, University at Albany, State University of New York

Reed, R. J. 1955 A study of a characteristic type of upper-level frontogenesis. *J. Meteorol.*, **12,** 226–237

Reed, R. J. and Danielsen, E. F. 1959 Fronts in the vicinity of the tropopause. *Arch. Meteorol. Geophys. Bioklimatol.*, **A11,** 1–17

Reed, R. J. and Sanders, F. 1953 An investigation of the development of a mid-tropospheric frontal zone and its associated vorticity field. *J. Meteorol.*, **10,** 338–349

Reed, R. J. and Albright, M. D. 1997 Frontal structure in the interior of an intense mature ocean cyclone. *Weather and Forecasting*, **12,** 866–876

Reeder, M. J. and Keyser, D. 1988 Balanced and unbalanced upper-level frontogenesis. *J. Atmos. Sci.*, **45,** 3366–3386

Roebber, P. J. 1993 A diagnostic case study of self-development as an antecedent conditioning process in explosive cyclogenesis. *Mon. Weather Rev.*, **121,** 976–1006

Rotunno, R., Skamarock, W. C. and Snyder, C. 1994 An analysis of frontogenesis in numerical simulations of baroclinic waves. *J. Atmos. Sci.*, **51,** 3373–3398

Sanders, F. 1988 Life history of mobile troughs in the upper westerlies. *Mon. Weather Rev.*, **116,** 2629–2648

1990 Surface analysis over the oceans—Searching for sea truth. *Weather and Forecasting*, **5,** 596–612

Sanders, F., Bosart, L. F. and Lai, C.-C. 1991 Initiation and evolution of an intense upper-level front. *Mon. Weather Rev.*, **119,** 1337–1367

Saucier, W. J. 1955 *Principles of meteorological analysis*. University of Chicago Press, Chicago, USA

Schultz, D. M. and Mass, C. F. 1993 The occlusion process in a midlatitude cyclone over land. *Mon. Weather Rev.*, **121,** 918–940

Shapiro, M. A. 1970 On the applicability of the geostrophic approximation to upper-level frontal-scale motions. *J. Atmos. Sci.*, **27,** 408–420

1976 The role of turbulent heat flux in the generation of potential vorticity in the vicinity of upper-level jet stream systems. *Mon. Weather Rev.*, **104,** 892–906

1981 Frontogenesis and geostrophically forced secondary circulations in the vicinity of jet stream–frontal zone systems. *J. Atmos. Sci.*, **38,** 954–973

1982 'Mesoscale weather systems of the central United States'. CIRES/NOAA Tech. Rep., Cooperative Institute for Research in Environmental Sciences, University of Colorado/NOAA, Boulder, CO 80309, USA

Shapiro, M. A. and Keyser, D. 1990 Fronts, jet streams and the tropopause. Pp. 167–191 in *Extratropical cyclones, The Erik Palmén memorial volume*. Eds. C. W. Newton and E. O. Holopainen. American Meteorological Society, Boston, USA

Staley, D. O. 1960 Evaluation of potential-vorticity changes near the tropopause and the related vertical motions, vertical advection of vorticity, and transfer of radioactive debris from stratosphere to troposphere. *J. Meteorol.*, **17,** 591–620

Stauffer, D. R. and Seaman, N. L. 1990 Use of four-dimensional data assimilation in a limited-area mesoscale model. Part I: Experiments with synoptic-scale data. *Mon. Weather Rev.*, **118,** 1250–1277

Uccellini, L. W. 1990 Processes contributing to the rapid development of extratropical cyclones. Pp. 81–105 in *Extratropical cyclones, The Erik Palmén memorial volume*. Eds. C. W. Newton and E. O. Holopainen. American Meteorological Society, Boston, USA

Uccellini, L. W., Keyser, D., Brill, K. F. and Wash, C. H. 1985 The Presidents' Day Cyclone of 18–19 February 1979: Influence of upstream trough amplification and associated tropopause folding on rapid cyclogenesis. *Mon. Weather Rev.*, **113,** 962–988

Zhang, D. and Anthes, R. A. 1982 A high-resolution model of the planetary boundary layer—Sensitivity tests and comparisons with SESAME-79 data. *J. Appl. Meteorol.*, **21,** 1594–1609